12-6-2023

Effect of Fabrication Pressure and NMC Cathode Composition on LPSCL Electrolyte for Solid-State Battery Performance Improvement

Winervil James
woj3921@g.rit.edu

ROCHESTER INSTITUTE OF TECHNOLOGY

Master Thesis

Effect of Fabrication Pressure and NMC Cathode Composition on LPSCL Electrolyte for Solid-State Battery Performance Improvement

Winervil James

A Thesis Submitted in Partial Fulfillment of the Requirements for the Degree of Master of Science in Mechanical Engineering

Department of Mechanical Engineering

Kate Gleason College of Engineering

Advisor: Dr. Isaac Perez Raya

Rochester Institute of Technology

Rochester, NY

December 6th, 2023

Thesis Committee

Dr. Matthew Ganter

Dr. Rui Liu

Dr. Robert Stevens

Abstract

Batteries are a key energy storage solution for a sustainable energy future. They provide carbon free power to portable devices such as mobile phones, laptops, and even electric vehicles. With further improvements to battery performance¸ the diversity of machines that can be electrified will increase. Solid state batteries (SSBs) have the potential to provide much greater energy density compared to conventional batteries. Greater energy density will help address the power to size ratio limitation of conventional batteries. Despite improvements in these major areas, SSBs still face some significant operational challenges. The study herein focuses on improving the performance of a full cell composed of an NMC (nickel-manganese-cobalt) composite cathode, sulfide solid electrolyte (lithium-phosphorus-sulfur-chloride), and a lithium metal anode. The cell performance was analyzed by changing the ratio of materials used in the composite cathode, which is made up of NMC, carbon black and the sulfide electrolyte material, LPSCL. In addition, the fabrication pressure of the cell was varied to identify conditions for stable cycling. Performance results showed that compared to other ratios a 60:35:5 percent split between NMC, LPSCL and carbon black showed a low resistance of 650 Ohms. In addition, a fabrication pressure of 25 MPa resulted in a long cycle time of 5 days with minimal decay in charge and discharge voltage. In order to better understand the fundamental principles behind the experimental results a battery model was created by customizing Ansys-Fluent with User-Defined-Functions (UDFs). The model was used to study the effect of contact resistance and ionic diffusion coefficient on the battery performance. The results of the model show that the diffusion coefficient affects the electrode utilization while the contact resistance influences the battery voltage. In particular, the results show that SSBs can be improved by ensuring that the contact resistance is less than the electrode resistance. Similarly, the high (350 MPa) and low (2.5 MPa) fabrication pressure test results show

a voltage limit of 3.8 V unlike the 25 MPa test. The voltage limit is indicated by the battery shorting, meaning that the contact resistance was greater than the electrode resistance. Another way to improve SSBs shown by the model is that by increasing the diffusion coefficient of the electrolyte, the cathode utilization will increase. Similarly, the 60:35:5 ratio cathode composition test showed low resistance, meaning that it is easier for ions travel to the cathode, resulting in greater cathode utilization.

Table of Contents

List of Figures

List of Tables

Nomenclature

cc	Concentration (mol/m^3)
DD	Diffusion coefficient (m^2/s)
ff	Electrode characteristic constant
FF	Faraday constant (96485.3 C/mol)
gg	Geometric factor
ii	Current density (mA/cm^2)
$\pi\pi$	Potential in electrode phase (Fermi potential) (V)
RR	Universal gas constant (8.314 J/mol-K)
rr	Electrode radius (m)
TT	Temperature (K)
tt	Time (s)
$\phi\phi$	Electric potential in the electrolyte (V)
XX	Dimensionless electrode concentration
yy	Cartesian coordinate yy (m)
zz	Cartesian coordinate zz (m)

Superscripts or Subscripts

ll	Electrolyte

ss	Electrode
-	Anion
+	Cation
*	Value at the electrode/electrolyte interface

Acronyms

CAM	Cathode active material
CCD	Critical current density
CEI	Cathode electrolyte interface
EIS	Electrochemical Impedance Spectroscopy
GCPL	Galvanostatic cycling with potential limitation
LE	Liquid electrolyte
LIB	Lithium-ion battery
LPSCL	Lithium phosphate sulfur chlorine
SOC	State of charge
SSB	Solid-state electrolyte
UDF	User Defined Function

1.0 Introduction

1.1 Relevance of Batteries

Batteries are an energy storage solution essential for today's society. Batteries are necessary for powering a majority of portable devices and are the driving force for enabling many technological advancements. As the world becomes electrified, the technical requirements of a single battery are becoming more robust [1]. This is especially true for applications such as collecting electricity from renewable sources and powering electric vehicles which require the ability to safely store and use large amounts of electricity. Currently, the best solution for these applications is lithium-ion batteries (LIBs) [2]. The introduction of LIBs in 1980 by John Goodenough represented a significant progression in battery technology [3]. Compared to previous prominent energy storage solutions (lead acid, zinc-carbon), LIBs are more compact and have higher energy storage capacity, improved safety, and the ability to be recharged. These characteristics made lithium ions batteries widely successful [4]. Advancements have produced many different form factors (cylindrical, prismatic, pouch) and sizes batteries to meet the needs of applications ranging from powering digital watches to storing megawatts of energy on a power grid [5].

Despite contemporary success, conventional LIBs are approaching their performance limit and are struggling to meet the demands of next generation technology without significant drawbacks in safety and size [6]. For this reason, recent research has gone into the development of solid-state batteries (SSBs). Viewed as the next leap in battery technology, SSBs utilize an alternative electrolyte, the solid-state electrolyte (SE) rather than the liquid electrolyte found in conventional LIBs. The SE offers benefits that directly counter the limitations of using a liquid electrolyte [7]. Compared to liquid electrolyte, the volume of solid electrolyte necessary to provide the same

energy density is much smaller. This will greatly reduce the size of an overall battery, allowing very high energy-dense batteries in manageable form factors [8]. Figure 1 shows the LIB on the left, the anode and cathode care submerged in the electrolyte solution, each cell produces 3.6 volts requiring 4 cells to equate SSB on the right which include a solid electrolyte and is more compact. A solid electrolyte also allows the stable use of lithium metal anodes whereas liquid electrolyte would corrode the lithium [9]. It is beneficial to use lithium metal as an anode because it provides the greatest energy density amongst other commonly used anode materials such as graphite and silicon, and it can be easily manufactured. Another prominent issue with conventional LIBs is flammability [10]. Conditions such as excessive heat and pressure can cause the liquid electrolyte to combust. Solid electrolytes have a much higher heat tolerance than liquid electrolytes which allows it to be more resistant to combustion and therefore safer [11]. The improved safety, size, and potential performance of SSBs make them a much-needed solution for increasing the range of electric vehicles and increasing the storage capacity of multi-gigawatt renewable energy farms. Improving clean energy generation and increasing SSB use in the transportation sector has the potential to significantly reduce pollution and its negative health effects [12]. Reducing pollution is a task that has become prominent in response to the aggressive net zero goal set by the UN in response to the pollution adverse climate effects that the globe has started to experience to global warming caused by pollution [13].

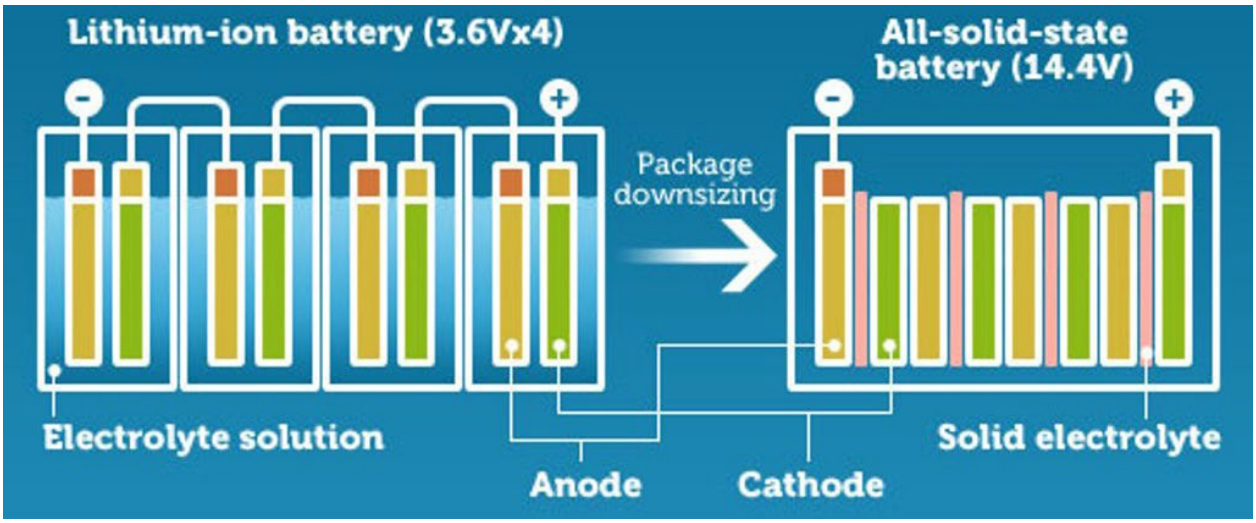

Figure 1: *Example of difference on package size of LIB and SSB.*

1.2 Main Issues to Overcome

Although there are several advantages to the use of SEs in solid-state batteries, there are still significant performance issues which are comparable with liquid electrolyte lithium-ion batteries. The main issue of concern is material instability [14]. The red boxes in Figure 2 highlight two consequences of material electrochemical instability. The two issues are, (i) dendrite growth and (ii) interphase growth, as discussed by Minnmann et al. [15]. In Figure 2, the top image magnifies the effect of dendrite growth occurring at the interface between the anode and solid electrolyte due to electrochemical instability. The magnified portion of the top image shows the beginning stages of dendritic growth. The jagged edges gradually lead to the formation of passageways through the electrolyte of a battery during cycling. These passageways are created over time as lithium metal from the anode accumulates at the anode-solid electrolyte interface and progresses through the electrolyte. Dendrites allow electrons to bypass the electrolyte and travel directly between the electrodes, thereby causing a short circuit [16]. In Figure 2, the effect of interphase growth at the

anode and SE interphase as a result of a chemical reaction is shown. The chemical reaction usually occurs due to an instability in the chemical bonds between the anode and electrolyte materials [17]. The green arrows in the bottom image of Figure 2 indicates the creation of a layer chemically distinct from the cathode or solid electrolyte. This layer takes up space previously filled by the cathode and solid electrolyte, causing a volume change of the battery cell and an increase in internal pressure [18]. The internal pressure created can accelerate dendritic growth by forcing the cracks that form at the anode further into the electrolyte. The right side of Figure 2 shows the compounded effect of interphase growth on the stack pressure. Stack pressure is an external pressure that is applied to the battery cell to keep the solid layers together and reduce contact resistance [19]. For SSBs the stack pressure can exceed 250 MPa. Such high pressure can greatly multiply the effect of a change in internal pressure. The ambiguous chemical makeup of the interphase layer can also negatively affect the conductivity of a battery by inhibiting the flow of ions to and from the cathode [20].

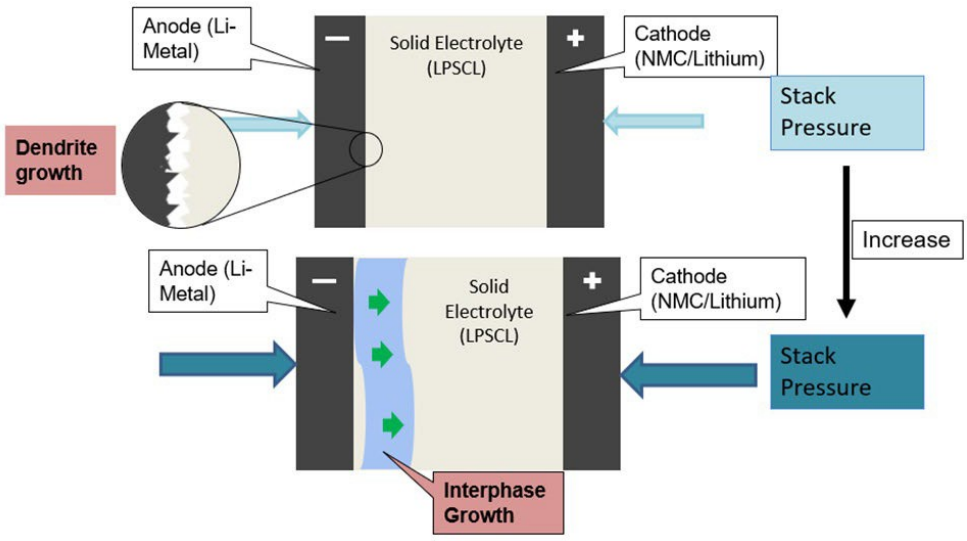

Figure 2: *Diagram of SSB challenges. Lithium metal dendrites grow through the SSE during discharge and cause the cell to short. High stack pressure encourages growth by forcing the lithium spikes further into the SE. Interphase growth is a chemical reaction which also occurs during discharge and causes volume increase and this stack pressure increase of the cell.*

1.3 Contribution of present work

Due to the emerging technology status of SSBs, there are not currently many reliable methods of studying interphase and dendrite growth [21]. For example, Han and colleagues sought to improve the electrochemical stability of their SSB by applying external compressive pressure of 20 MPa during cycling [22]. However, this method did not capture the effect of the battery cell fabrication pressure prior to cycling at 20 MPa. The full cell fabrication pressure is important because it is the first factor that affects the contact between the solid layers of the battery cell. This is especially significant for the lithium anode and SE interface which is where dendrite growth can be expedited by high pressure. A separate study done by Minnmann's group indicated that a composite cathode active material ratio of 70 percent will provide high energy density while minimizing interphase growth [15]. However, this number was not supported by experimental results and no reasoning was given for why different ratios would not be as effective. This work proposes a way to better understand and interpret the interfacial phenomena of dendrite and interphase growth by conducting a study to expand on the factors that affect SSB performance including cathode composition, fabrication pressure, and other more fundamental parameters (e.g., contact resistance and ionic diffusivity). The contributions of the present work are:

1) Identifying the influence of composite cathode materials ratios on the cell current flow resistance of a SSB by using electrochemical impedance Spectroscopy (EIS).

Different combinations of composite cathode and electrolyte material have shown to have desirable stability over longer cycle. One such example is a sulfur based solid electrolyte such as LPSCL (lithium-phosphorous-sulfur-chloride) in combination with NMC (nickel-manganese-cobalt) composite cathode made up of NMC, LPSCL, and carbon black [23]. By optimizing the

amounts of material in the NMC composite cathode for the LPSCL pellet being tested, a best-case ratio for stability and performance can be found. In this study it was found to be a percent ratio of 60:35:5 (NMC, LPSCL, carbon black) with a complete cathode mass of 10 g. The best-case ratio was able to achieve a minimum resistance of 380 ohms.

2) Identify the influence of cell fabrication pressure SSB cycle time by conducting experiments with galvanostatic cycling with potential limitation (GCPL).

When solid state batteries are created, it is necessary to apply pressure to the cell stack to ensure the solid layers, including the cathode, SE, and anode have the best possible contact. While this pressure is necessary, applying too much can damage the cell. The point of contact for applying the pressure is the cathode. Excess pressure can cause the cathode to crack and lose contact with the solid electrolyte, creating areas of high contact resistance and low cycling stability. Therefore, several tests were performed at different fabrication pressures to measure the current flow resistance. The results showed that a fabrication pressure of 25 MPa had the longest cycle at over five days with minimal decay in charge and discharge voltage, indicating the cell could maintain performance.

3) Developing a simulation model for identification of the fundamental electrochemical reactions and transport processes in a battery.

A complementary model of a solid-state battery was created through Ansys-Fluent customization to explore the connection between contact resistance and the electrolyte ionic diffusion coefficient. Through this model, a starting point for better understanding the relationship between the stack pressure, contact resistance and ionic diffusion of SSBs can be established.

2.0 Literature Review

This section describes a brief review of the work completed by researchers relating to performance evaluation of SSBs and the related areas for improvement. This first part of the review is broken down into the solid components of the battery. Section 2.1 provides background on cathode materials that have been used for SSBs. Section 2.2 covers factors affecting solid electrode material selection. Section 2.3 introduces the concerns of external pressure on battery cell performance. Section 2.4 contains papers relating to lithium-ion battery modelling.

2.1 Cathode

In order to maximize the extremely high capacity of a lithium metal anode [24], it is necessary to maximize the cathode capacity. Studies suggest that the cathode active material (CAM) type and content in the cell are what ultimately determine the maximum capacity of the cell. Composite cathodes are viewed as a solution to capacity matching [25]. A composite cathode is made of a CAM and solid electrolyte (SE) material in combination with polymer binders and carbon-based additives which improves mechanical and electrical properties, respectively [26]. Figure 3 shows the structural condition of elements at the cathode, particle and interface level. Each level has conditions that result in inhibiting cathode functionality. For instance, a notable condition is percolation pathways which are synonymous with dendrites and can cause shorting by allowing a direct connection between the anode and cathode [27].

There have been some viable compositions (Sb_2S_3–LPS–AB) which have been successfully studied for stability [28]. In this example, the CAM is antimony trisulfide (Sb_2S_3), the solid electrolyte material is lipopolysaccharide (LPS), and the binder is acetylene black. In order to improve stability, it is important to accurately balance the volume fraction of the CAM with

electrode thickness. Currently, ease of ionic transport is guaranteed by an approximate 50 volume percent CAM fraction. Other suggestions (60 & 70 vol%) vary depending on active surface area and porosity of the composite mixture [15].

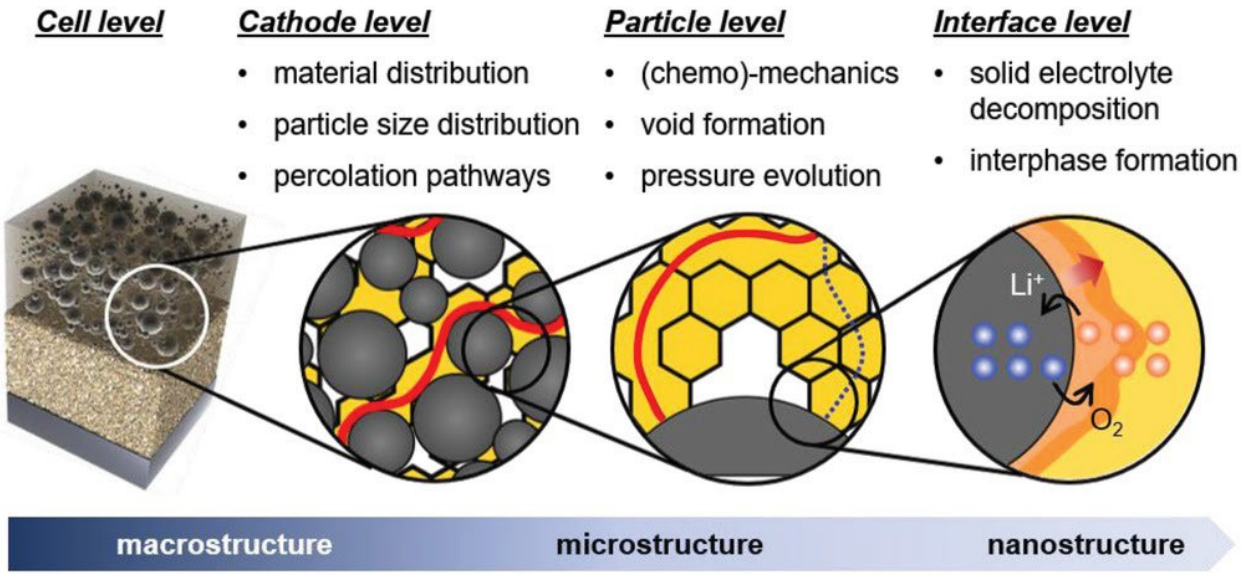

Figure 3: *Schematic overview of the processes occurring on different length scales in SSB cathodes, caused by poor matching of tailored materials properties. Image adapted from Minnmann et al* [15].

During cycling, (electro-)chemically driven volume or morphology changes of the cathode are characterized by chemo mechanical changes in the CAM [29]. Figure 4 shows the mechanical and chemo mechanical challenges that come into play when using a solid electrolyte vs. a liquid electrolyte. As indicated in Figure 4c, changes such as the expansion/contraction of the CAM have a more severe implication of contact loss between the solid layers for SSBs (Figure 4b). In addition, volume changes result in large anisotropic stress and mechanical damage to the cathode. Therefore, there is a need to understand the effect of (chemo-)mechanical processes on battery performance and to find strategies to mitigate this degradation mechanism.

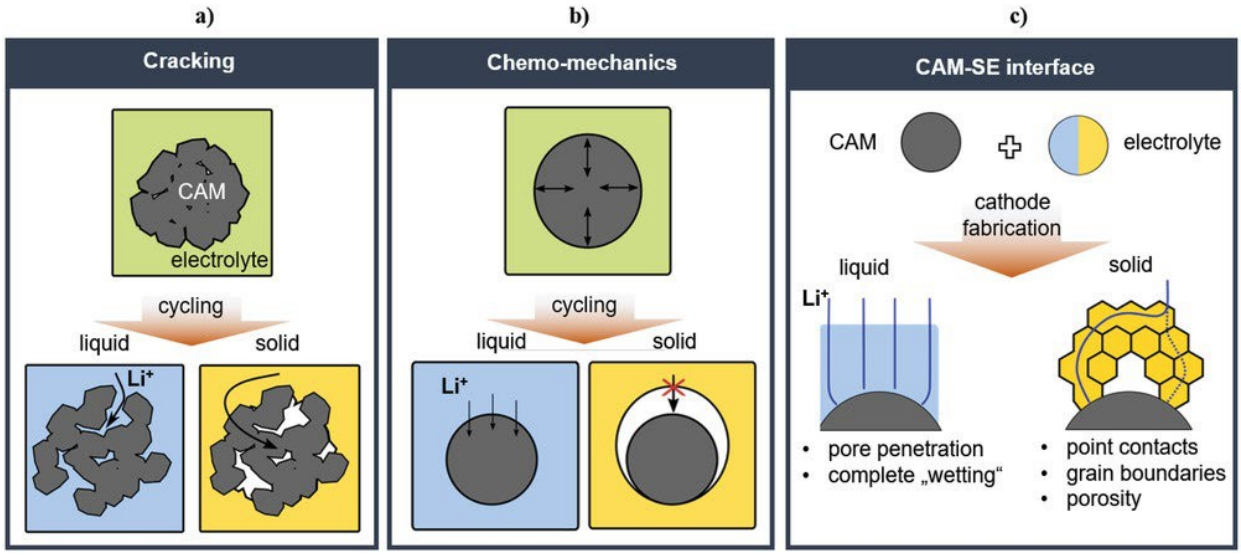

Figure 4: *Schematic illustration of effects that come into play if changing the liquid electrolyte to a solid electrolyte. Image adopted from Minnmann et al [15].*

The combination of CAM nickel cobalt manganese (NMC), solid electrolyte material lithium-phosphate-sulfur-chloride (LPSCL), and carbon black has been found to allow electro-chemically driven volume changes during battery operation up to a comparably moderately high degree. This capability is due to the high ionic conductivity and mechanical property (malleability) of Li-thiophosphate SEs [30].

The lack of chemical compatibility between CAMs and SEs will result in oxidation of the SE. Oxidation of the SE is detrimental to the ionic conductivity of the conductive phases that form at the cathode-SE interface. In the case of thiophosphate-based SE, oxidation phases such as phosphites/phosphates, sulfites/sulfates, and polysulfides restrict ionic transport routes leading to increased interfacial resistance [31].

Other than switching to more stable SE materials (Halide, oxides) adding a protective layer to prevent contact of the CAM with SE is one viable solution. However, certain layers don’t allow

enough electron transport for de-lithiation while maintaining proper contact between cathode and SE during morphological changes (Oxides) and can be expensive (halides). This is a unique challenge that emerging research in Organic battery electrode materials (OBEM) has begun to address [32].

2.2 Solid Electrolyte

The majority of publications concerning Li dendrite formation has been done primarily on symmetric Li/Li electrode cells or "half cells" [33]. The interfacial phenomena that cause filament growth likely differ substantially for full cell applications. Therefore, there is a need to build on the current characterization techniques in order to develop more realistic mitigation strategies.

Li filaments through SEs are detrimental to SSB by causing decrease in efficiency and eventually cell failure. The current density at which a Li filament propagates across a SE is known as the critical current density (CCD) [34]. CCD is dependent on the critical stack pressure applied on a cell which aids in mitigating pore formation during Li stripping and thus preventing percolation of Li into the SE. The effect of critical stack pressure is especially significant to symmetric cells where Li plating and stripping occur simultaneously. This is not the case for full cells, which may indicate that lower stack pressure can create the same dendrite mitigation effect.

Figure 5 shows the different factors that can affect cathode functionality. As indicated in the figure, Li filament growth at the SE interface is dependent on the electrolyte's transference number, the electrolyte's mechanical properties, and Li-metal impurities (Figure 5c). Although it has been shown that increasing SE shear modulus and making transference number less than unity help defend against Li filament formation, neither method completely prevents it.

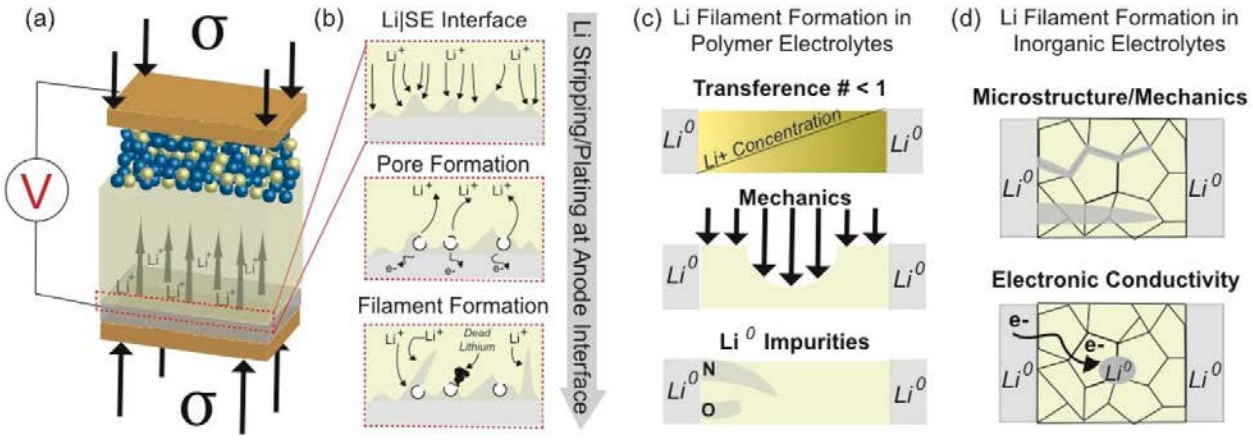

Figure 5: *Full cell battery structure with pressure (σ) applied to the cell (a). The characteristics of the Li/SE interface controls ionic flux, pore formation in the Li-metal upon stripping, and Li filament growth (b). Li filament growth is controlled by electrolyte mechanics, transference number, and the presence of interfacial impurities (c). Li filaments in inorganic SEs are identified with electronic conductivity, microstructural properties, and interfacial contact (d). Adapted from Hatzell et al. [33].*

It has been demonstrated that Li filament propagation favors pre-existing microstructural inconsistencies in SE material. Subsequent work showed that Li growth preferred the electrode edge (current focus areas) over mechanical defects. This is an electrolyte defect contributing to the inconsistency of CCD values for Li-metal SSBs [35].

The majority of SEs form an interphase at Li metal interface due to redox reactions. An interphase that:

- Conducts both ions and electrons will continue to grow over time since it is fueled by the direct electrochemical reaction occurring at the SE.
- Conducts only ions grow to a set thickness, which can result in a stable layer.
- Has insufficient ionic conductivity will cause increased impedance.

This characterization of the interphase is made possible by in situ and operando experimental observation using instruments such as X-ray photoelectron spectroscopy (XPS), scanning and

transmission electron microscopy (STEM/TEM) and Electron energy loss spectroscopy (EELS) [36].

The most prominent class of present-day SEs are sulfide-based materials, or in particular lithium thiophosphates, displaying exceptionally high ionic conductivities up to 2.2 mS cm−1 [37]. They also have suitable mechanical properties (i.e., malleability and low Young's modulus), which initially makes them ideal candidates. However, they exhibit a narrow electrochemical stability window, which highlights the necessity of matching the electrolyte with a stable composite cathode.

2.3 Stack Pressure

Optimal stack pressure in the megapascal-level is said to be needed for optimal solid state battery performance [38]. The stack pressure, which is a uniaxially applied external force is required to maintain contact at the interface of the electrodes and solid electrolyte and promote ionic conductivity [39]. Continued research has been conducted to explore the relationship between the mechanical behavior of the interfacial materials used in SSBs [40]. There are also challenges faced with the use of a solid interface [19].

Han and his group were able to analyze stack pressure. The result of this study established that a positive relationship exists between high stack pressure (1-200 MPa) depending on the SE material and composite cathode. While this pressure is lower than other studies, there is still concern that the internal stress/strain generation in the cathode from stack pressure can cause cracking of the SE matrix (including the separator layer). This negatively affects the ionic and electronic percolation pathway promoting dendrite growth. The end result is poor electrochemical

reversibility and capacity fading due to loss of contact to CAM with prolonged cycling [22].

Figure 6 shows cycling performance of cells at the stack pressure of 50-76, 250 and 350 MPa. As indicated in the figure it is possible to reduce stack pressure to tens of megapascals (50-75 MPa) while maintaining electrochemical performance as shown by the capacity curves in figure. The results from Ye et al. suggest that it is possible to maintain interfacial contact and minimize contact resistance at stack pressures below hundreds of MPa [41].

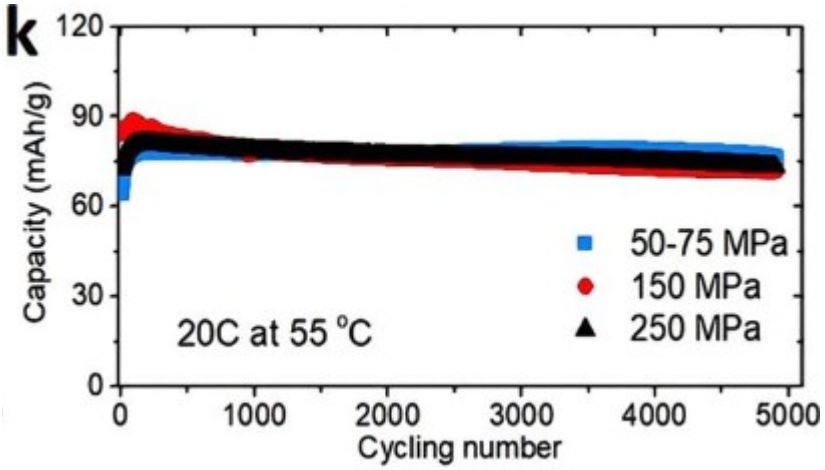

Figure 6: *Cycling performance of solid-state battery with multilayer electrolytes under different operating pressures of 50–75 MPa, 150 MPa and 250 MPa. Adapted from Ye et al. [41].*

A widely used method of measuring stress in composite materials is the use of optical signals. Blanquer et al. used these sensors to monitor stress by placing the optical sensor between the cathode and SE. Another test was done by placing the optical sensor between the anode and the SE (Solid Electrolyte) under cycling pressure [42]. The results of the study indicate that external sensors are not able to accurately capture (internal) stresses at the electrode level during cycling. Based on this result it can be said that the external stack pressure could correlate to even larger internal pressure, which is not beneficial to prolonged battery cycling.

2.4 Battery Model

West et al. [43] focuses on the modeling of porous insertion electrodes in the presence of electrolytes. The areas studied are the interactions between electrode structure, electrolyte diffusion, and electrochemical reactions. Figure 7 shows Wests' electrode model. It consists of electrodes suspended in an electrolyte. The small vertical arrows indicate the direction of ion diffusion, and the large horizontal arrow in the center is the concentration gradient of the model.

The study is conducted by using an approach that combines macroscopic transport equations, microscopic electrochemical kinetics, and computational simulations [44]. The macroscopic level is concerned with the transport of ions within the porous electrode structure, accounting for variables such as electrode porosity and the electrolyte concentration gradients. The macroscopic level is integrated with microscopic reaction kinetics, focusing on charge transfer rates and their dependence on the electrode's porosity.

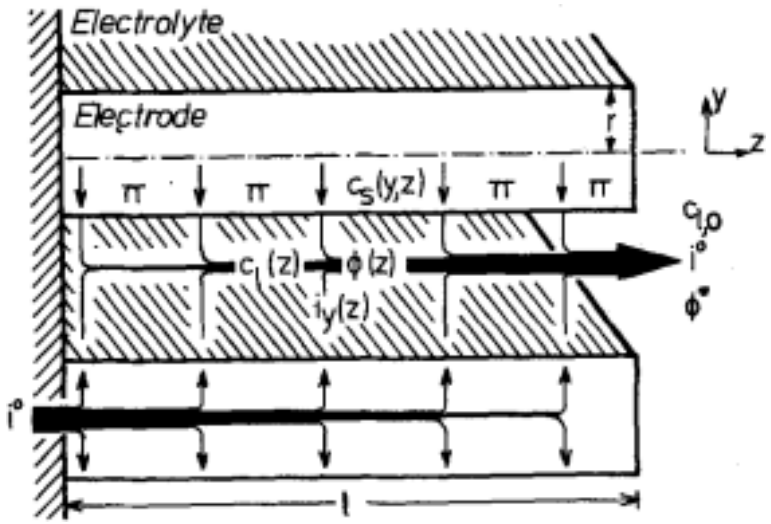

Figure 7: *Schematic diagram of electrode model (plane geometry). Arrows indicate the direction of fluxes considered. Give the image a title and at the end of the title. Adapted from West et al. [43].*

A key finding of the paper is the optimal electrode porosity range. The electrode porosity range helps establish efficient ion transport and effective charge transfer. This is due to the influence of porosity on both ion diffusion and electrochemical reaction rates [45]. Porosity can also be linked to cell external stack pressure. The connection is that higher pressure creates lower porosity and lower pressure, greater porosity [46]. This has implications for the design and performance of efficient battery systems in terms of how porosity, or stack pressure is controlled during prolonged operation.

Experimental data can be used to drive a battery model [47]. Doyle and colleagues combined experimental data and modeling to provide insights into the behavior of lithium/polymer/insertion cells [48]. This was done by using a mathematical model to describe the electrochemical processes occurring during galvanostatic charge and discharge cycles of the insertion cell. The model accounts for ion transport within the polymer electrolyte, the kinetics of insertion reactions at the electrode-electrolyte interfaces, and the influence of electrode porosity and thickness.

Previously collected experimental data was used to validate and correct the model. This was done by matching the model parameters with the experimental behavior of the cell in order to increase the accuracy of the model's results.

Fuller et al. explored techniques to further optimize models of dual lithium ion insertion cells [49]. The different areas covered in the study were the electrode materials, electrochemical reactions, and transport phenomena within the cell. Computational simulations and optimization algorithms were used to better define parameters such as electrode thickness, porosity, and particle size distribution are considered.

Based on the conclusions made concerning electrode morphology, optimal cell configurations can

be created [50]. The cell configurations can be designed to maximize energy density, power density, or cycle life. Ultimately, the findings from this model can help advance the development of more efficient battery systems by optimizing cell function and making performance predictable.

3.0 Hypotheses and Objectives

3.1 Hypotheses

The issues challenging the development of solid-state batteries are chemical and mechanical in nature. In order to address these issues, target areas for the current study were identified. The interaction of the solid materials in the battery is related to how well ion transport can be maintained over a period of time. An enabling factor of ion transport is how well the solid surfaces can maintain contact to allow the necessary electrochemical reactions to occur. The following proposed hypothesis were identified in the present study:

(i) Solid material ratio composition affects battery resistance influencing performance. Electrochemically unstable cathode and electrolyte combinations have shown poor performance. Improving the chemical stability between the solid electrolyte and cathode material is one path forward to better battery performance.

(ii) Fabrication pressure affects cycling stability. Cell fabrication pressure influences long term cyclability of battery cells. Excess pressure could damage the cell resulting in contact loss.

(iii) Ion diffusion coefficient affects battery performance. The diffusion coefficient is a parameter directly related to the ability of ions to travel in the electrolyte. A higher diffusion coefficient will increase the ion mobility directly influencing the depletion of ions in the electrolyte and the usage limits of the electrode active material.

(iv) Contact resistance affects the performance of the battery.

The contact between electrode/electrolyte has shown to be a primary factor affecting the performance. A contact resistance may lead to a drop in the concentration influencing the battery voltage or current discharge.

3.2 Objectives

Solid state batteries require improvement in electrochemical and electromechanical stability. In order to achieve this, it is important to first improve the composition of the cathode for better compatibility with the solid electrolyte. Further improvements lie in the potential for higher ionic conductivity through increasing the ion diffusion coefficient, and more sustainable performance by decreasing contact resistance. As a result, this project focuses on three main objectives:

Objective 1: Optimize composite cathode material composition for reducing battery current flow resistance.

Objective 2: Determine NMC composite cathode fabrication pressure to increase battery cell cycle time.

Objective 3: Create battery model to analyze the effect of parameters such as ion diffusion coefficient and contact resistance on battery performance.

4.0 Methods

4.1 Experimental Methods

This section describes the methods used for fabrication of materials used in testing and the assembling and use of the test setup. Section 4.2 provides details on material acquisition for the cathode and solid electrolyte. Section 4.3 covers the steps for assembly of the test cell. Section

4.3.1 details how the SSB cell is assembled in the test setup. Section 4.3.2 explains how data is collected from the test setup. Section 4.4 covers the parameters being test which are the full cell fabrication pressure and composite cathode material ratios.

4.2 Material Acquisition

The materials necessary for testing are LPSCL (lithium-phosphorus-sulfur-chloride), NMC (nickel-manganese-cobalt), and Nano Carbon black. LPSCL, the solid electrolyte material was chosen to be used due to high ionic conductivity when compared to other solid electrolyte materials (cite paper review). Similarly, the cathode material (NMC) was chosen for its stability with LPSCL, proven through testing (section 5.1). Nano carbon black is a necessary component for making the NMC composite cathode. It is known as a binder material which means it helps maintain the connection between the cathode active materials and conductive additives. For an NMC composite cathode the active material is NMC and the conductive additive is LPSCL (cite lit. rev.). The anode material used for all testing was lithium metal. All materials were purchased as quality-controlled powders from the material supplier MSE supplies.

4.3 Test Preparation

The following steps were completed before assembling the experimental test setup:

- Determine the amount of precursors (NMC, LPSCL, Carbon black) that need to be mixed in the mortar then weight out the precursors and add to the mortar. Mix for 5 minutes.
- Then make a SE pellet in the small peek tube using approximately 50 mg of SE and applying a pressure of 300-500 MPa and cold press for 2 minutes.
- Put the small metal rods in with the SE and measure the thickness of SE using the caliper

and record that value and zero the caliper again.

- Then add desired amount (10/40 mg) of composite cathode from the mortar to the small peek tube and press at 350 MPa (*Figure 8*).

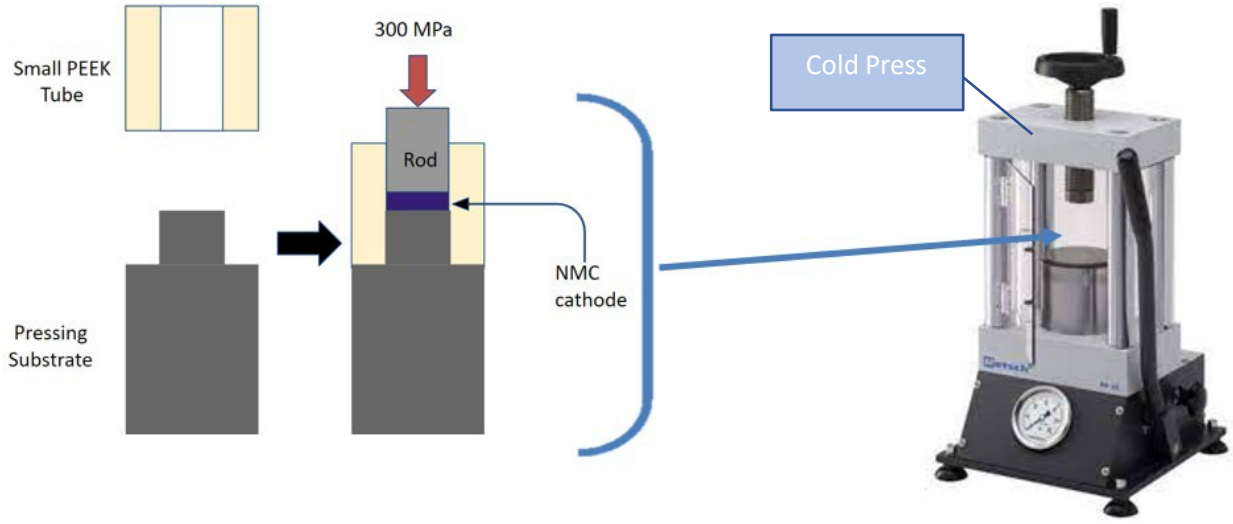

Figure 8: *Process of making NMC composite cathode. Material is filled into the small peek tube then pressed.*

- Put the small metal rods back in the peek tube and measure the thickness of the cathode. Record the value.
- Then, roll out a lithium granule into a sheet, and hole punch it to make a lithium metal anode.
- Apply anode to one of the copper current collectors, then place the two current collectors on two sides of the battery, the current collector with the lithium metal goes on the anode side, the current collector without the lithium metal on the cathode side.
- Assemble the battery test setup in the order shown in the diagram below (4.3.1).

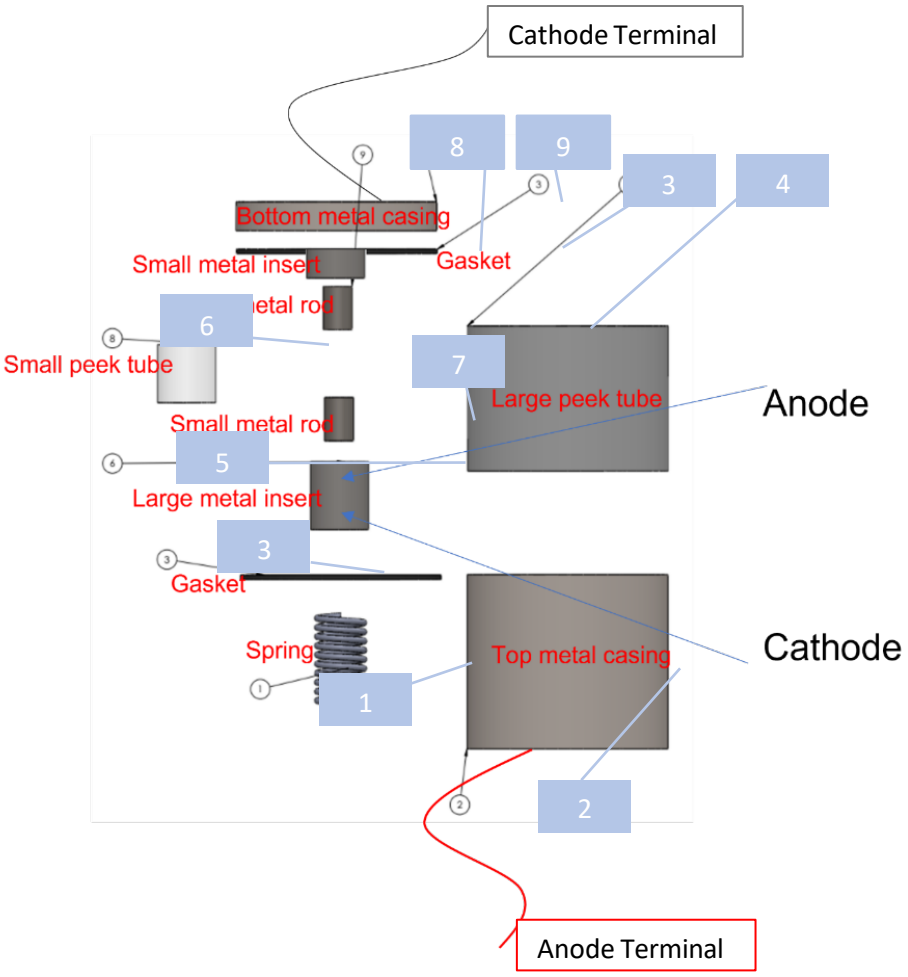

Figure 9: *Order that the test setup should be assembled (1-10).*

4.3.1 Battery Assembly

The battery is assembled in a stacked manner, the order is indicated by the numbered items 1-10 in Figure 9. Starting from component one, the spring is placed into the center of the top metal casing (2). Then, a gasket (3) is placed onto the top of the metal casing. Next, the large peek tube (4) is placed on top of the gasket. The large metal insert (5) is then placed inside the large peek tube followed by the small peek tube (6) with the small metal rods (7) inserted into each end. The small metal insert (8) is then placed on top of the small peek tube assembly. The final two components are another gasket (3) which rests on top of the large peek tube (4) and the bottom

metal casing (9) which is placed on top of the gasket. Once stacked the bottom and top metal casing are screwed together.

The cell is held in a small peek tube (Figure 9, *#8*) and stack pressure is applied by the spring rod. The spring rod is forced onto the anode interface of the cell by the spring (Figure 9, #1) which is compressed when the setup is fully assembled. A control rod contacts the cathode interface and prevents the pellet from being pushed out of the small peek tube. Wires are run from the top and bottom metal casings that serve as the anode and cathode terminal as indicated by the red and grey lines leaving the casing in Figure 9.

4.3.2 Experimental Testing

The wires from the two terminals connect to the VSP-300 (Figure 10) which produces EIS (Electrochemical Impedance Spectroscopy) and galvanostatic (cycling) data for each cell configuration via EC lab software. The EIS is an indication of the ionic conductivity of the cell and galvanostatic cycling indicates how long the cell takes to charge and discharge over a period of time. These performance metrics are examined in more detail in the results section.

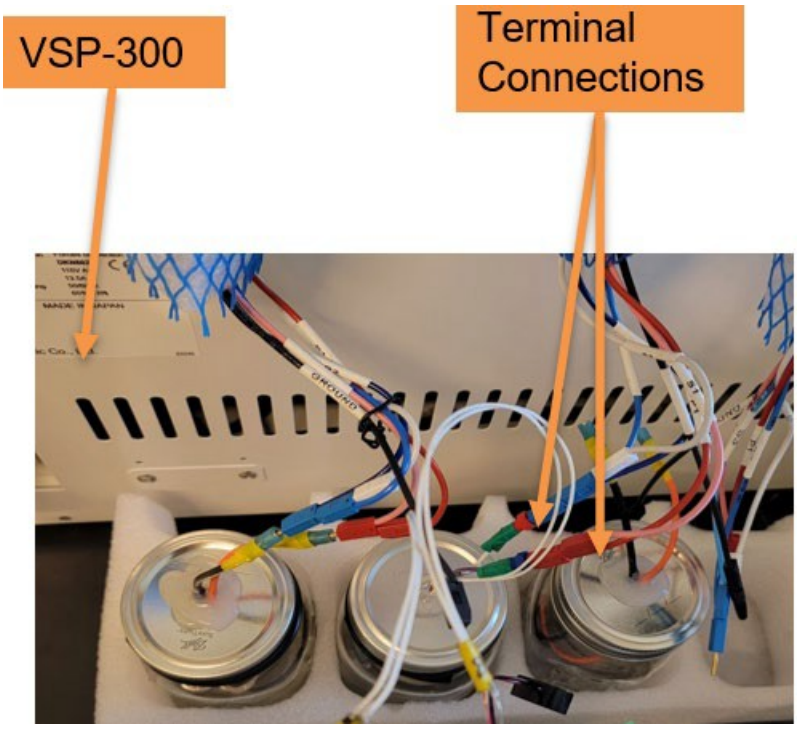

***Figure 10**: Test device connections for test setup*

4.4 Cathode optimization

In order to improve the performance, it is necessary to find the optimal ratio of composite cathode materials. Section 4.4.1 explores specific ratios of cathode active material (CAM), conductive, and binder material to improve the current flow resistance of the NMC cathode. In addition to this, section 4.4.2 test different full cell fabrication pressures to improve the consistency for stable cycling. Each modification stems from the general cathode preparation process detailed in section 4.3.

4.4.1 Material Ratio

An NMC composite cathode cell was tested at reference conditions with the NMC cathode. The goal was to achieve regular battery performance before attempting to achieve NMC cathode improvements. The NMC composite cathode was mixed and pressed according to the procedure in section 4.3, Figure 8. For this experiment, the reference percent ratio of cathode materials used was, NMC:LPSCL:Carbon black = 76:19:5. That is, for a total NMC composite cathode mass of 40 mg there was 30.4 mg NMC, 7.6 mg LPSCL, and 2 mg carbon black. In order to test material ratios with a lower amount of NMC, two additional ratios were tested. The ratios tested were 76:19:5 and 60:35:5 (Table 1) as percentages of a total composite cathode weight of 10 mg. Each of the ratios were tested twice to confirm the result. Also, each of the ratios were tested separately at different times with a freshly fabricated solid electrolyte and lithium metal anode cell.

Table 1: *Ratios tested for NMC cathode.*

Experiment	Ratio (NMC:LPSCL:Carbon black)
1	76:19:5
2	60:35:5

4.4.2 NMC Cathode Fabrication Pressure

Next, full cell fabrication pressure was measured as shown in Table 2. Fabrication pressure refers to the amount of pressure that was applied to press the cathode into the solid electrolyte during assembly of the battery cell. For each of the tests #1-3, the given full cell fabrication pressure was tested twice to confirm the result. The fabrication pressure for test #4 was only tested once given the positive cycling results. Each of the ratios were tested separately at different times using a 10 mg cathode with a freshly fabricated solid electrolyte and lithium metal anode cell. The purpose of changing this pressure is to find the best pressure at which contact with the current collectors is promoted without damaging the weak constitution of the relatively powdery composite cathode.

Table 2: *Fabrication Pressure and time for composite cathode optimization*

Test	Fabrication Pressure (MPa)
1	350
2	50
3	2.5
4	25

4.5 Battery Model to Identify Effect of Diffusion Coefficient and Contact Resistance

4.5.1 Computational Domain, Governing equations, and boundary conditions

The procedures below will cover the steps taken to create the battery model. The model used is based on a lithium ion battery model created by the West et al. [43]. It was modified and then used to produce results for the effect of the ion diffusion coefficient and contact resistance on battery performance.

The 1D model consists of two regions, the porous electrode regions and the electrolyte. Each region is defined by governing equations and boundary conditions that describe the diffusion of ions across them and

thus the performance of the battery.

Figure 11 shows a schematic of the battery model consisting of (i) cathode electrode rods, and (ii) electrolyte. In addition, Figure 11 shows the boundary conditions in the electrode and electrolyte.

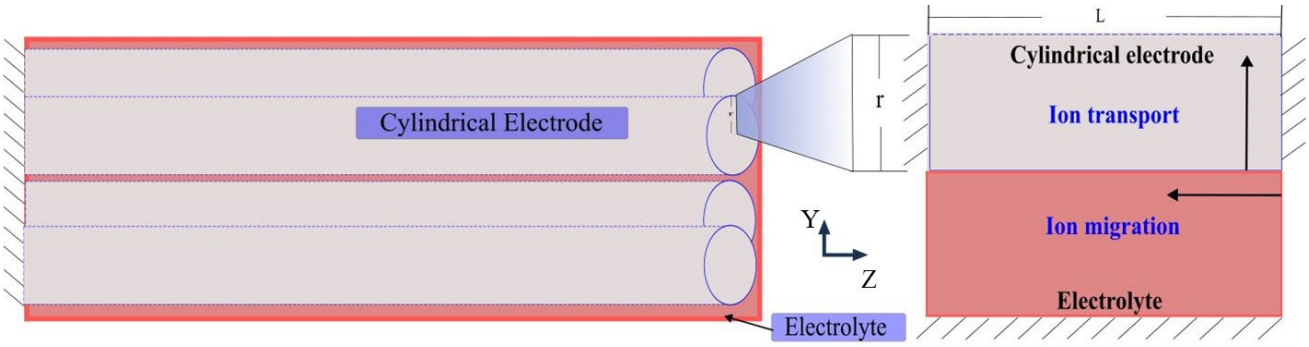

***Figure 11**: Schematic of electrode model*

At the cathode electrode, the inserted lithium ions (generated at the by the electrochemical reaction at the interface electrolyte/electrode) transport through the electrode. Eq. (1) governs the diffusion process.

$$\frac{\partial \partial cc_{ss}}{\partial \partial tt} = DD_{ss}\frac{\partial^2 cc_{ss}}{\partial y^2} \tag{1}$$

where cc_{ss} is the concentration of the inserted specie in the electrode, tt is time, DD_{ss} is the diffusion coefficient, and yy is the Cartesian vertical coordinate. The electrode particle has a symmetric condition at the center $yy = 0$ (it is assumed to be a cylinder). Also, at the electrode/electrolyte contact $yy = rr$, the inserted specie depends on the current density. Eqs. (2) and (3) show the boundary conditions for the electrode.

$$\frac{\partial cc_{ss}}{\partial yy}\Big|_{yy=0} = 0 \tag{2}$$

$$\frac{\partial \partial cc_{ss}}{\partial \partial yy}\Big|_{yy=rr} = -\frac{ii}{FFDD_{ss}} \tag{3}$$

where ii is the current density across the particle/electrolyte interface, and FF is the Faraday constant. The initial conditions assume that the electrode is in equilibrium with a saturated electrolyte and a non-utilized electrode.

$$cc_{ll} = cc_{ll,0} \tag{4}$$

$$cc_{ss} = cc_{ss,0} \tag{5}$$

$$\phi\phi = \phi\phi^{0} \tag{6}$$

At the electrolyte, the positive and negative ions follow one-dimensional diffusion and migration according to Nerst-Planck transport equation, Eqs. (7) and (8). Also, electro-neutrality enforces the condition of equal anion and cation concentration.

$$\frac{\partial\partial cc_{ll}}{\partial\partial tt} = \frac{\partial\partial}{\partial\partial zz}DD_{-}\left(\frac{\partial\partial cc_{ll}}{\partial\partial zz} - cc_{ll}\frac{FF}{RRTT}\frac{\partial\partial\phi\phi}{\partial\partial zz}\right) \tag{7}$$

$$\frac{\partial\partial cc_{ll}}{\partial\partial tt} = \frac{\partial\partial}{\partial\partial zz}DD_{+}\left(\frac{\partial\partial cc_{ll}}{\partial\partial zz} + cc_{ll}\frac{FF}{RRTT}\frac{\partial\partial\phi\phi}{\partial\partial zz}\right) + \frac{iigg}{FF} \tag{8}$$

where cc_{ll} is the positive or negative ions concentration in the electrolyte, DD_{-} is the diffusion coefficient of the anions, DD_{+} is the diffusion coefficient of the cations, RR is the universal gas constant, TT is the temperature, $\phi\phi$ in the electric potential in the electrolyte, and gg is a geometric factor between the circumference and the crosssectional area of the pore. The boundary conditions for the electrolyte are zero flux at $zz = 0$ and constant concentration and potential at the opposite side (electrolyte concentration is constant far from the electrode surface).

$$\frac{\partial\partial cc_{ll}}{\partial\partial zz}\Big|_{zz=0} = \frac{\partial\partial\varphi}{\partial\partial zz}\Big|_{zz=0} = 0 \tag{9}$$

$$cc_{ll}(ll) = cc_{ll,0}; \quad \phi\phi(ll) = \phi\phi^{*} \tag{10}$$

where $cc_{ll,0}$ is the initial concentration of the electrolyte, and $\phi\phi^{*}$ is the equilibrium electrode potential.

In the electrolyte, the potential depends on the local surface concentration of the ions in the electrode and

electrolyte. Eq. (11) shows the dependence equation utilized by West et al. [43].

$$\pi\pi - \phi\phi = (\pi\pi - \phi\phi)_0 + \frac{RRTT}{FF}\left(\ln\left(\frac{cc_{ss}^{0} - cc_{ss}^{*}}{cc_{ss}^{*}}\right) + \ln(cc_{ll}) - ff\left(\frac{cc_{ss}^{*}}{cc_{ss}^{0}}\right) - 0.5\right) \quad (11)$$

where $(\pi\pi - \phi\phi)_0$ and ff are characteristic constants of the electrode material, and cc_{ss}^{*} is the concentration of ions in the electrode at the surface.

Table 3 shows the values of the electrochemical properties adopted for modeling. The values come from West et al. [43]. Having similar values allows a straight comparison between the reported results and simulation results with the developed model for verification purposes. In addition, it is important to indicate that the simulated model is non-dimensional and therefore the values may not be primary factors influencing the results (dimensional parameters drive the modeling of the battery).

***Table 3**: Simulation parameters (values obtained from West et al. [22])*

Parameter	Value	Unit
Transport data, electrolyte:		
Anion diffusion coefficient (DD_{+})	1.61×10^{-6}	cm^2/s
Cation diffusion coefficient (DD_{-})	6.45×10^{-6}	cm^2/s
Transport data, electrode:		
Lithium diffusion coefficient (DD_{ss})	10×10^{-10}	cm^2/s
Geometrical data:		
Electrode thickness (ll)	0.05	Cm
Particle diameter (rr)	5×10^{-5}	Cm
Porosity	0.35	
Discharge current density	5	mA/cm^2
Electrolyte concentration (start) ($cc_{ll,0}$)	1×10^{-3}	mol/cm^3

Saturation concentration of electrode ($cc_{ss,0}$)	2.5×10^{-2}	mol/cm^3

4.5.2 Utilizing the simulation model to evaluate effect of diffusion coefficient

The simulation was conducted with various diffusion coefficients to evaluate the effect on the battery performance. The values were decreased and increased from the reference value reported by West et al. of $DD_{+,\mathrm{ref}} = 1.61\times10^{-6}$ cm^2/s [43]. The evaluated range was $DD_{+,\mathrm{ref}}/20 \le DD_{+,\mathrm{ref}} \le 20DD_{+,\mathrm{ref}}$.

4.5.3 Utilizing the simulation model to evaluate the effect of contact resistance

The simulation model was modified to show the impact of contact resistance on battery performance. The contact resistance was determined by using the electrode resistance as a reference. In the dimensionless space, the electrode diffusion coefficient is UU_{ss} with a diameter YY. The total resistance offered by the electrode is then:

$$RR_{ss} = \frac{YY}{UU_{ss}} \tag{12}$$

A contact resistance of 25% means that $RR_{cc} = 0.25RR_{ss}$. In the proposed approach, the contact resistance leads to a concentration jump at the contact between the electrolyte and electrode. The jump in the concentration is governed by the flux condition at the contact Y = 1.

$$\nabla_{YY} XX|_{YY=1} = \frac{\Delta CC}{RR_{cc}} \tag{13}$$

where ΔCC is the drop in the concentration. It is important to observe that in the proposed approach, the contact resistance has no impact on the flux condition at the contact, which comes from assuming conservation of transport of the inserted species in the electrode. The drop in concentration affects the potential E that influences the ions transport and the battery voltage.

4.5.4 Ansys-Fluent Customization for Battery Modeling

Technical literature distinguishes various approaches to analyze batteries utilizing commercial software. These approaches analyze batteries from different perspectives. Simulations in Ansys-Fluent mainly focus on gaining understanding of the thermal processes (e.g, battery cooling, thermal stresses, and heat generation for different types of materials). Chen et al. [51] utilized Ansys-Fluent to investigate the battery the effect of cooling techniques on the battery temperature, energy, and weight. It was found that indirect liquid cooling system leads to the lowest temperature rise. Mačák et al. [52] investigated the electric potential and temperature distribution in a lithium-sulfur battery by coupling a subscale electrochemical model to the Dual Potential Multi-Scale Multi-Domain (MSMD) in Ansys-Fluent. By determining curve-fitting battery modeling parameters, results indicated good agreement between a 0D MATLAB model and the simulation results for different battery performance curves. Parmar et al. [53] utilized MSMD in Ansys-Fluent and identified that the greater contributor to heat generation was the ohmic heat generation in a lithium ion battery pack. Cai and White [54] utilized the battery model in COMSOL to investigate the performance of a lithium battery and identified that higher cell temperatures lead to higher cell voltages during the discharge process.

Currently, an out-of-the-box Ansys-Fluent software lacks a suitable battery model capable of modeling the fundamental ionic transport process and the interaction between the electrolyte and electrode. However, a fundamental model was necessary to for accurate battery representation, which is essential to identify the intrinsic mechanisms in the battery storage and discharge processes. Creating a model through customization not only addressed the immediate needs of a functional model for battery analysis, but also gave a path to gain fundamental understanding of

the battery working principles. Therefore, the present work required more than just inputting parameters or values into a graphics user interface. The developed battery model required tailoring Ansys-Fluent to incorporate the general governing transport equations and the reactions adding ions into the electrode and consuming cations and anions in the electrolyte. The following lines describe the way the software was customized to enhance the overall functionality of the software and achieve the simulation of a lithium battery.

Figure 12 shows a schematic of the computational domain and grid in the battery modeling. The simulation considers two computational domains (i) electrode and (ii) electrolyte. The two domains are connected at the interface electrode/electrolyte. The computational grids consist of multiple square cells. Each cell has a face and a cell center. At the interface on the electrolyte side, the lithium cations are consumed at a rate proportional to the battery discharge current. At the interface on the electrode side, the lithium ions go into the electrode at a similar rate.

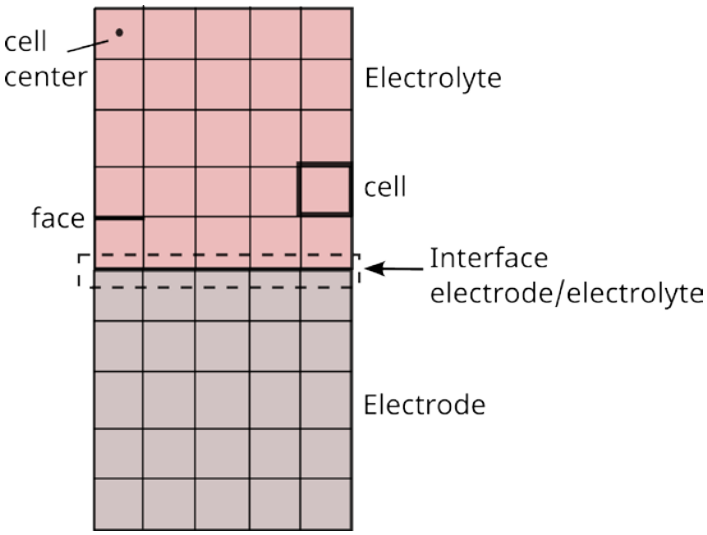

***Figure 12**: Computational domain and mesh in the battery modeling along with relevant terminology.*

The battery modeling requires including the governing equations for the transport of ions in the electrode Eq. (1) and the transport for the ions in the electrolyte Eqs. (7)-(8). An out-of-the-box

Ansys-Fluent does not contain the governing equation of the transport of ions in the electrolyte. To add the equation, a user-defined scalar (UDS) can be customized. Eq. (14) is the UDS for diffusion transport of concentration in Ansys-Fluent.

$$\frac{\partial \partial cc_{ll}}{\partial \partial tt} + \frac{\partial \partial}{\partial \partial zz} \left(-\Gamma \frac{\partial \partial cc_{ll}}{\partial \partial \partial \partial} \right) = SS \tag{14}$$

Eq. (14) in Ansys can transform into Eq. (8) for the electrolyte ionic transport by making SS in Eq. (14) becomes:

$$SS = \frac{\partial \partial}{\partial \partial zz} DD_{+} \left(cc_{ll} \frac{FF}{RRTT} \frac{\partial \partial \phi \phi}{\partial \partial zz} \right) + \frac{iigg}{FF} \tag{15}$$

The transport of anions in the electrolyte Eq. (7) follows a similar approach with declaration of source terms. Also, the transport of ions in the electrode Eq. (1) is also modeled through a UDS in Ansys-Fluent by making the source term equal to zero.

The customization for the ionic transport in the electrolyte can be done by utilizing the source term in the UDS. The source term can be controlled with a user-defined function.

A user-defined function, or UDF, is a C function designed to enhance Ansys-Fluent standard features. In the present battery model, the UDFs compilation allowed:

(i) declaration of source terms in the general transport equations to solve non-conventional equations.

(ii) execute commands at the end of each iteration to calculate the potential effects in the electrolyte

(iii) execute commands at the end of each time-step save data of the solution of equations

The UDFs use predefined macros in Ansys Fluent to perform specific tasks such as

(i) looping over all the computational cells

(ii) retrieve properties stored at the center of computational cells (e.g, ionic concentration)

(iii) perform efficient operations (e.g., vector operations for potential gradient calculation, and identification of cells in the electrolyte or electrode domains)

Table 4 shows the macros utilized in the present study to generate the battery model in Ansys-Fluent. It also shows the functionality of the UDF in the model and the specific task conducted by the macro. Figure 13 shows the framework of the developed C functions. The main framework consists of five UDFs. The UDF DEFINE_INIT assigns the initial conditions of concentration to the electrode and electrolyte. The UDFs DEFINE_ADJUST visit the electrode and electrolyte to extract or assign the information related to the cell potential required to calculate the potential term in the transport equations (electrolyte ionic transport). Finally, the UDF_SOURCE assigns the potential terms as a source term in the transport equations (electrolyte ionic transport). User Defined Memories (UDMI) are utilized to memorize information on the calculations of each UDF and share it with other UDFs. Looping macros (c_loop and f_loop) allow visiting the computational cells centers and faces.

***Table 4**: Ansys-Fluent macros utilized to model battery ionic transport and performance.*

DEFINE Macro	Function	Required for (specific task)
UDF DEFINE_INIT	Assign values	Definite initial concentration in electrode and electrolyte
UDF DEFINE_ADJUST	Manipulate variables	Extract electrode concentration from faces at the interface

		electrode/electrolyte
UDF DEFINE_ADJUST	Manipulate variables	Calculate potential
UDF DEFINE_ADJUST	Manipulate variables	Calculate potential gradients
UDF DEFINE_SOURCE	Declares source terms	Define potential term in electrolyte
C_UDMI(c,t,0), UDM0	Memorize information in cells	Share electrode concentration between UDFs
C_UDMI (c, t,1), UDM1	Memorize information in cells	Share potential concertation between UDFs
C_UDMI (c, t,2), UDM2	Memorize information in cells	Share gradient of potential (second derivative) between UDFs
begin_c_loop	Loop over cells of electrode and electrolyte	Assign initial concertation
begin_f_loop	Loop over boundary faces of electrode	Extract electrode concentration, store in UDM0
begin_c_loop	Loop over cells of electrolyte	Read UDM0 with electrode concentration, calculate potential, store in UDM1
begin_c_loop	Loop over cells	Read UDM1 with potential and calculate second derivative
c_face_loop	Loop over the faces of a cell (connectivity macro)	Extract electrode concentration in neighboring cells

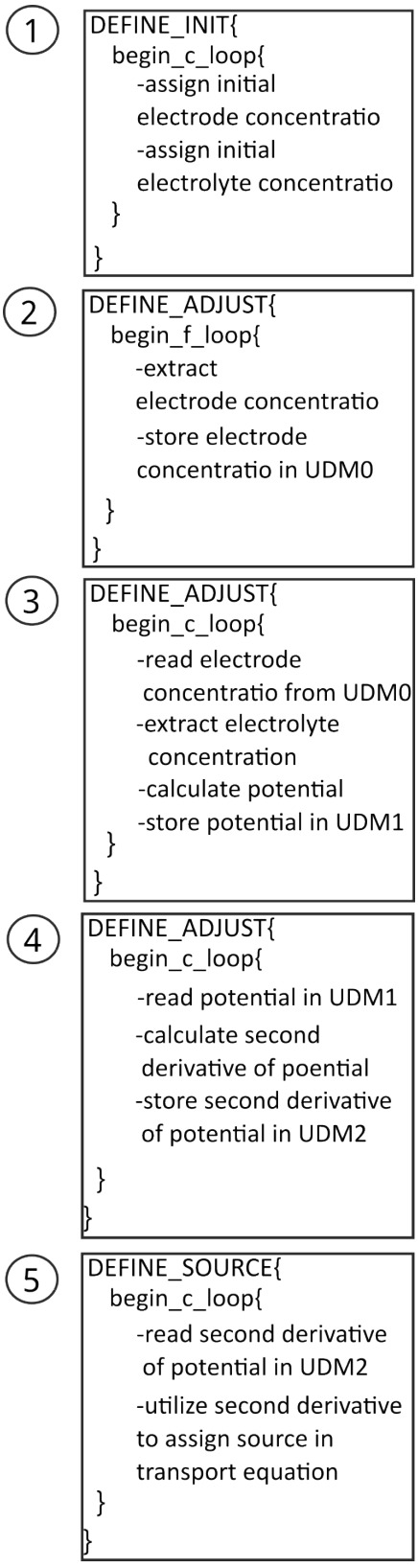

***Figure 13**: Flow process of programmed functions in C (UDFs) to customize Ansys for battery modeling.*

The calculation of the second derivative in the source term required the application of central differences approximation. The figure shows a computational domain with multiple cells. As shown in Figure 14, Each cell can be represented as a cell with center at P and faces at “w” and “e.”

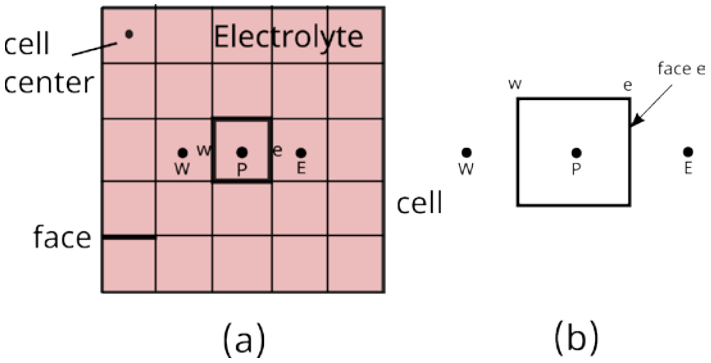

Figure 14*: Schematic of computational domain with relevant grid terminology in 1D modeling. (a) Electrolyte with multiple cells. (b) Individual cell P with neighboring cells W and E.*

The second derivative in a given cell P, requires knowing the values of the concentration at the cells W and E. Perez-Raya and Kandlikar [55] give detailed documentation on theory of finite volume for numerical approximation of first and second order derivatives in 1D models. The source term at cell P used for the calculation of the second derivative is by:

$$SS_{pp} = DD_{+}\frac{FF}{RRTT}\left(cc_{ll_{ee}}\frac{(\phi\phi_{EE}-\phi\phi_{PP})}{\Delta zz}\frac{1}{\Delta zz}-cc_{ll_{ww}}\frac{(\phi\phi_{PP}-\phi\phi_{WW})}{\Delta zz}\frac{1}{\Delta zz}\right) \quad (16)$$

At the cells in contact with a boundary, first term approximation (forward or backward differences) was adopted for the gradient calculation. The calculation of the potential second order derivative required the customization of Ansys-Fluent. Connectivity macros allowed visiting the neighboring cells (E, W) for each cell P in the computational grid. Figure 15 shows the programing frame necessary to calculate the source term in Eq. (16).

```
DEFINE_ADJUST{
  begin_c_loop{
  -Read potential in UDM1
      c_face_loop{
           -Get potential at cells
           W, P, and E
           -Get electrolyte
           concentratio at faces e, w
            -Calculate second
            derivative of poential
           -store second derivative of
           potential in UDM2
      }
 }
}
```

Figure 15*: Flow process of programmed functions in C to calculate and store the second derivative of potential.*

Figure 16 shows the process in the customized software Ansys-Fluent to model the ionic transport and performance of the lithium battery. The process is as follows:

Step-1: start with initializing the concentration in the concentration in the electrode and electrolyte (box-1 in Figure 13)

Step-2: Ansys-Fluent solves equation for electrode concentration (lithium ions diffuse into the electrode; ions added to the electrode at a rate proportional to the discharge current through the boundary condition Eq. (3))

Step-3: Extract concentration on the electrode surface (box-2 in Figure 13)

Step-4: Extract electrolyte concentration (box-3 in Figure 13)

Step-5: Calculate battery potential (box-3 in Figure 13)

Step-6: Calculate second derivative of potential (box-4 in Figure 13 and box in Figure 15)

Step-7: Assign second derivate as a source term into the ion transport electrolyte equation (box-5 in Figure 13)

Step 8: Ansys-Fluent solves equation for electrolyte concentration (lithium cations and anions diffuse into the electrolyte; cations and anions consumed at a rate proportional to the discharge

current through the source term Eq. (15))

Step 9: Ansys-Fluent checks for convergence (convergence means Ansys-Fluent found the solution to the ion transport equation in the electrolyte with the corresponding boundary conditions and added source term)

Step 10: If convergence has not been satisfied, go to step 5.

Step 11: Save electrode concentration, and cell potential in a text file.

Step 12: If (i) convergence has been satisfied, (ii) electrolyte is not depleted, and (iii) electrode still has active material, increase the time by a time-step and go to Step-2.

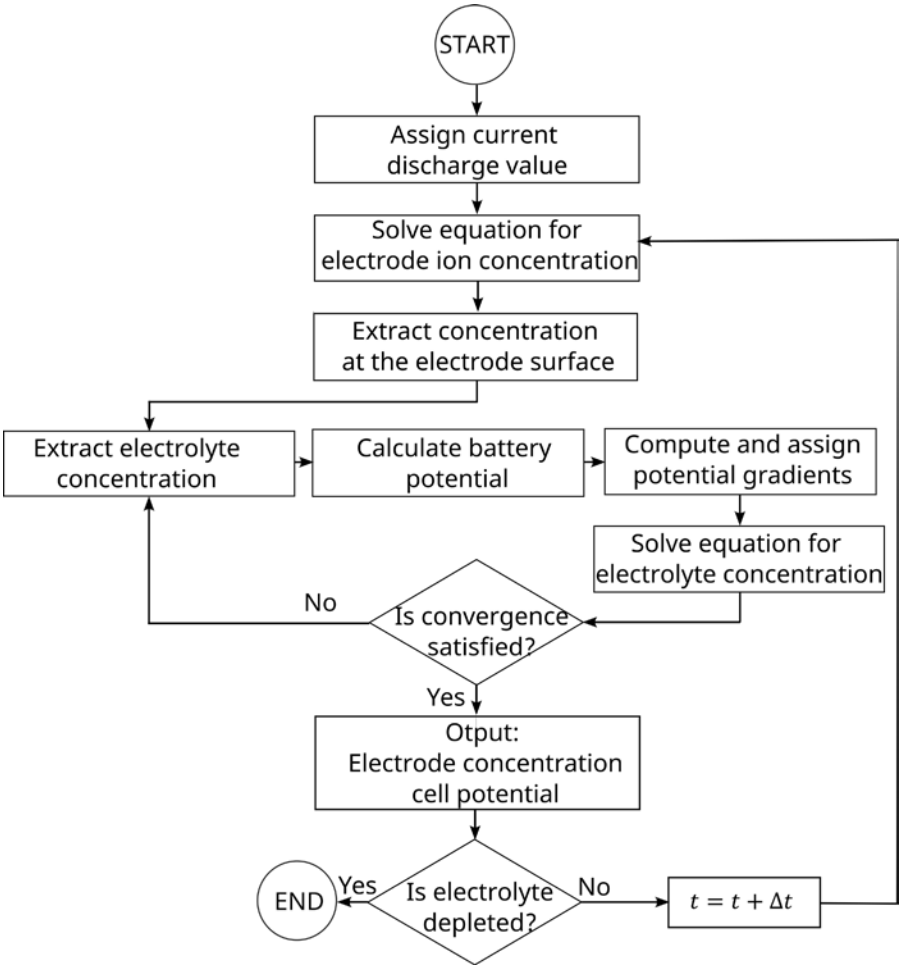

***Figure 14**: Flow chart of computer modeling of the lithium battery in Ansys-Fluent.*

5.0 Results

This section shows the results obtained for the analysis of the battery. Section 5.1 focuses on testing hypothesis 1, which regards changing the cathode composite material composition to achieve a low resistance cell. Section 5.2 focuses on testing hypothesis 2, which regards modifying cell fabrication pressure to increase total cycle time. Finally, section 5.3 discusses the results of the modeling developed to test the effect of diffusion coefficient and contact resistance on the battery performance (hypothesis 3 and 4).

5.1 Results: Material Ratios

The graph below shows the EIS performance of an NMC composite cathode test with a material percent ratio of 76:19:5 (NMC:LPSCL:Carbon black) making up a 40 mg cathode. The minimum point of the curve in **Error! Reference source not found.** indicates that the NMC cathode had a current flow resistance of about 380 ohms.

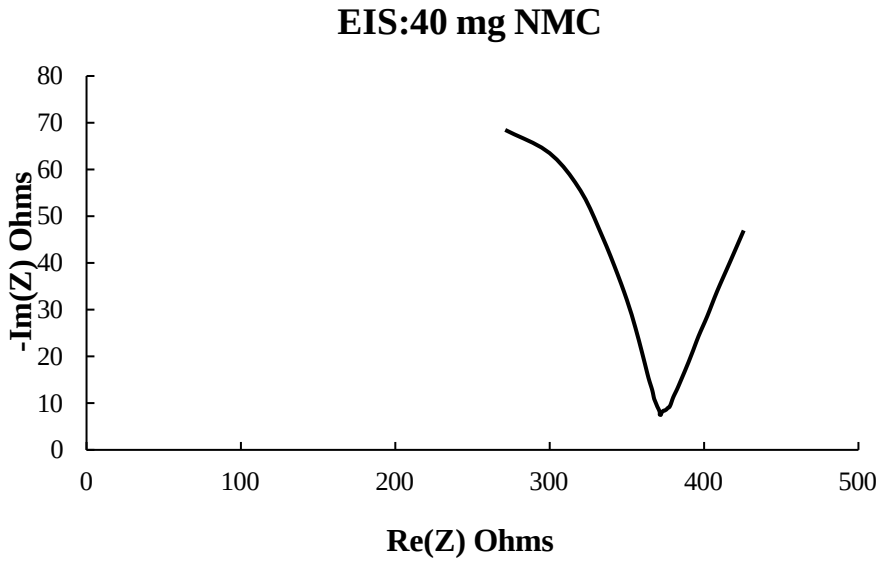

Figure 12: *EIS results of 40 mg NMC composite cathode cell*

To determine the best cathode ratio for testing, two additional composite cathode ratios were tested. The percent ratios of NMC:LPSCL:Carbon black were 76:19:5 (ratio #1) and 60:35:5 (ratio #2) each making a 10 mg cathode. The metric for evaluation was the EIS test which is an indication of cell current resistance. From the two EIS tests shown, it is clear that 60:35:5 is the better ratio out of the two. The resistance shown in Figure 13 is about 200 ohms higher than the resistance shown in Figure 14 which is about 700 ohms. This indicates that for a 10 mg cathode, ionic conductivity is better with a slightly lower amount of NMC (CAM) and more conductive additive (LPSCL). Out of all three tests, the 40 mg cathode had the lowest resistance of 480 ohms.

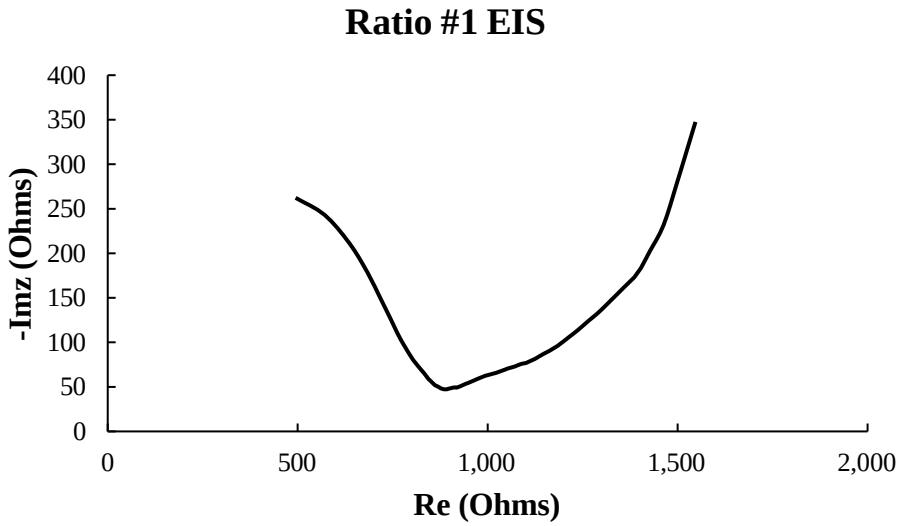

***Figure 13**: EIS test indication stack resistance for cathode ratio #1*

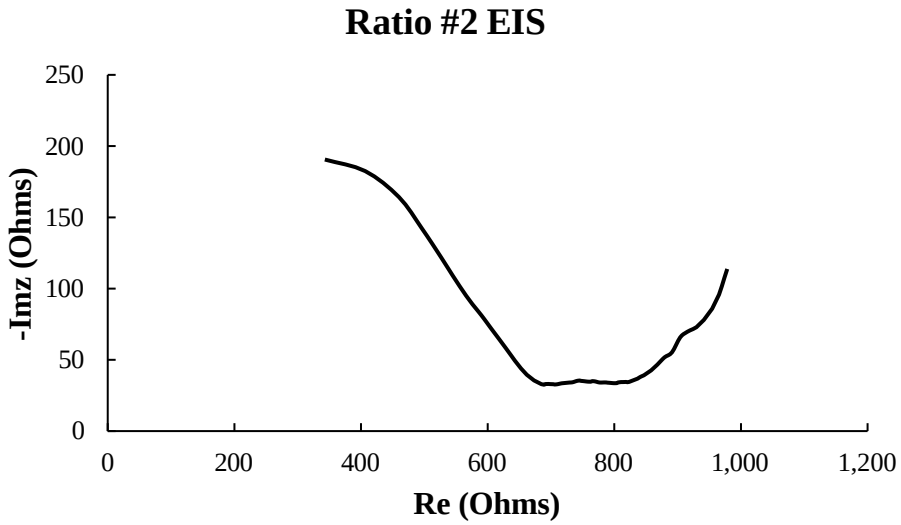

***Figure 14**: EIS test indication stack resistance for cathode ratio #2*

5.2 Results: Cathode Optimization

Full cell fabrication pressure was tested next. To create a reference, the 40 mg NMC composite cathode was cycled with no fabrication pressure (Figure 15). The results show that the NMC cathode cell is able to cycle in the voltage range indicated by the clear increase (charge) and decrease (discharge) curves that it goes through. However, there is a large amount of cycling decay indicated by the increasing steepness of the curve cycles over time.

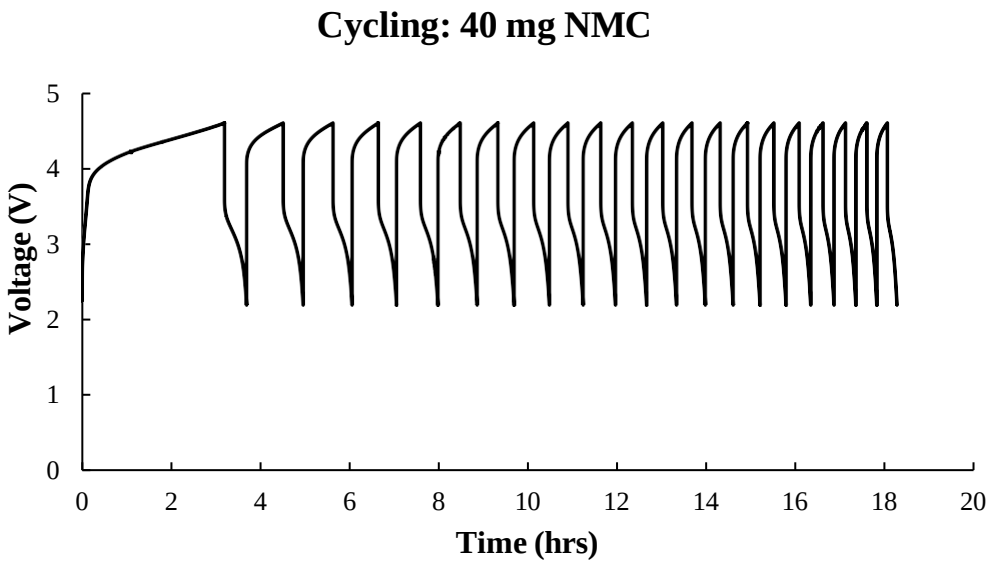

Figure 15: *Cycling results of 40 mg Lithium and NMC cathode cell.*

Continuing with the 60:35:5 percent ratio, four full cell fabrication pressures were tested. The purpose was to determine which pressure encouraged int resulted in the best cycling performance. The graphs below show the cycling results of the tests from **Error! Reference source not found.**. Comparing Figure 16 and Figure 17, it is clear that test 1 had a cycle time about 6 hours shorter than test 2. This indicates that lower full cell fabrication pressure results in longer cycle time. Both tests soft shorted during charge and were not able to discharge.

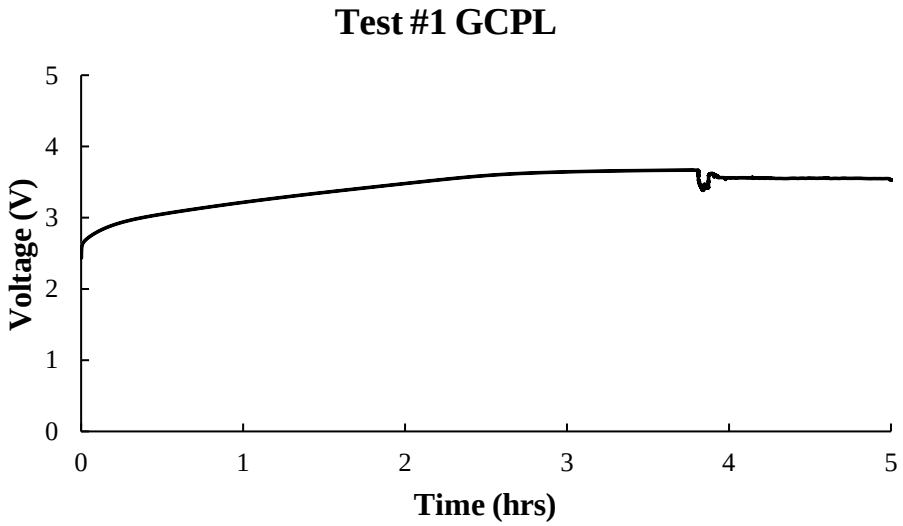

***Figure 16**: GCPL indicating cycle time and voltage for Test #1*

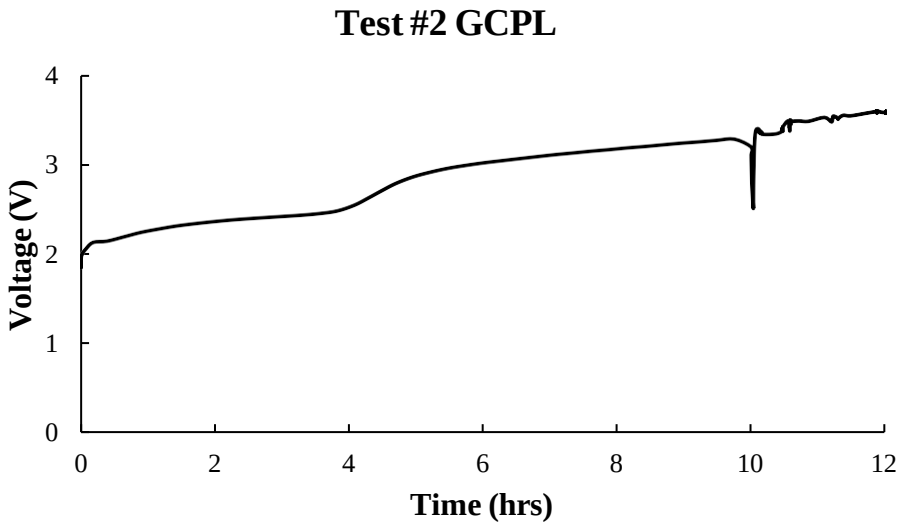

***Figure 17**: GCPL indicating cycle time and voltage for Test #2*

Next, a low full cell fabrication pressure of 2.5 MPa was used for test #3 (Figure 18). The result is that the cell shorted after about 2.7 hours of charge. This is about hour shorter than the cycle time of test 1 and 7 hours shorter than test 2. The performance of test 3 indicates a lower limit for full

cell fabrication pressure. Likewise, test 1 indicates a high limit for full cell fabrication pressure. Given these limits, the final test used 25 MPa for full cell fabrication pressure. The cycling results of 25 MPa was significantly better than the other tests.

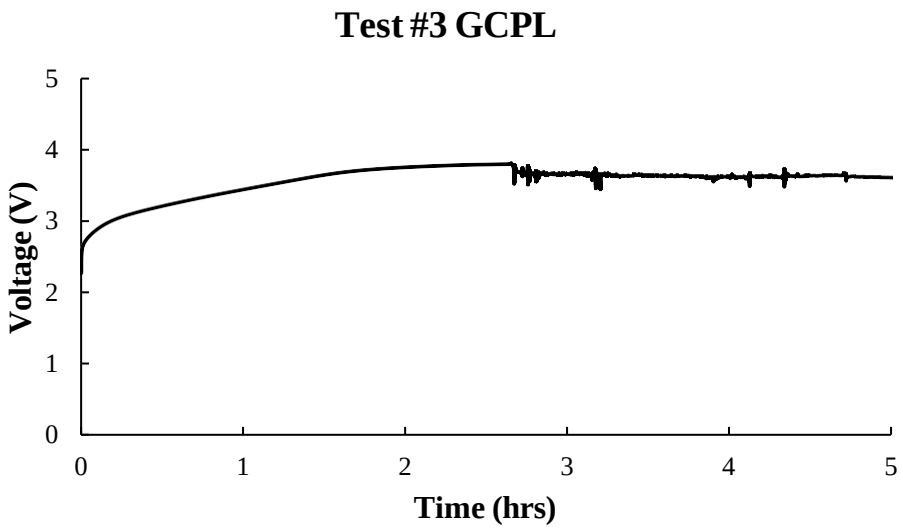

***Figure 18**: GCPL indicating cycle time and voltage for Test #3*

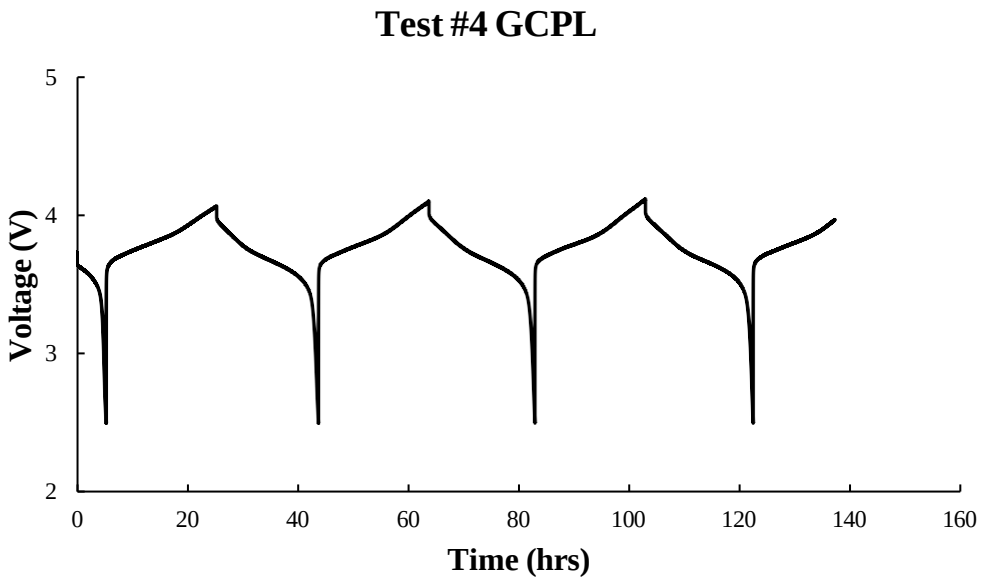

Figure 19: *GCPL indicating cycle time and voltage for Test #4*

As shown in Figure 19, test 4 cycled for 140 hours or 5 and a half days. This is a great improvement over the previous maximum cycle time of around 10 hours from test 2 (Figure 17). Unlike the other tests (except 40 mg), test 4 was able to complete several full charge and discharge cycles. The maintenance of symmetry in the charge (increase) and discharge (decrease) of the curve indicates minimal cycle decay. This means that if the cell is electrochemically stable and could continue to reach the charge and discharge voltage to provide reliable energy. This is a better result that the 40 mg cathode test (Figure 15) which would provide almost no power after 16 hours due to cycle decay. Despite the 40 mg cathode having higher conductivity (Figure 12), the cycling performance is much worse than the 10 mg cathode that was tested (Figure 19).

5.3 Simulation Results

The main purpose of the simulation is to achieve a better understanding of the fundamental transport and reaction processes occurring in a battery. In addition, the developed simulation can be utilized to evaluate the influence of relevant parameters driving the battery operation. The following sections evaluate the accuracy of the developed model by direct comparison with the results reported by West et al. [43], and identify the effect of the diffusion coefficient and contact resistance. The discharge current remains constant and equal to 4.2 mA/cm^2.

5.3.1 Verification of the accuracy of the simulation results

Figure 20 compares the performance curve obtained from the conducted simulation by customizing Ansys-Fluent with the curve reported by West et al. [43]. The y-axis shows the potential and the x-axis shows the dimensionless concentration $XX = cc_{ss}/cc_{ss,0}$. At the initial condition, the concentration X is zero and the potential is 2.42 V. As the battery discharges, the potential decreases and the electrode concentration increases. The process continues until (i) the ionic concentration in the electrolyte becomes zero (depletion of the electrolyte is reached), or (ii) the ionic concentration in the electrode becomes one (the electrode becomes saturated). Results show similar decay in the performance curves with a slight over-prediction of the voltage by the developed model. In addition, the results indicate that both models (West and proposed) predict a fully depletion of the electrolyte when the electrode has reached concentration close to 80% utilization.

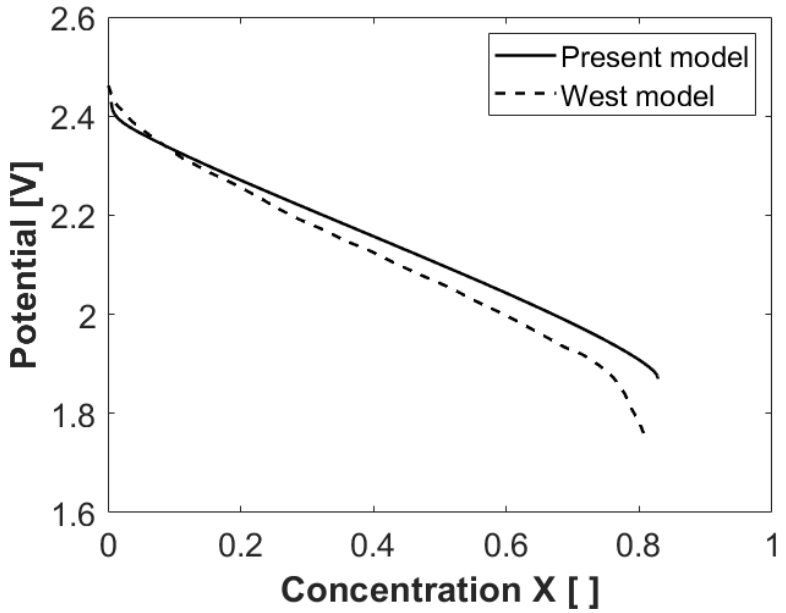

Figure 20: *Comparison of battery performance obtained with the developed simulation and the simulation results reported by West et al [22].*

5.3.2 Diffusion Coefficient

Figure 21 shows the simulated performance curves for the analyzed range of the diffusion coefficient. Results indicate that the diffusion coefficient has a strong influence in the electrode utilization. The increase in the diffusion coefficient results in an augmented utilization of the electrode. An increase in the diffusion coefficient leads to more mobility of the ions in the electrolyte. The stronger diffusion allows more ions to reach the electrode region, which delays the depletion of the electrolyte. Results show the change in the diffusion coefficient (in the analyzed range) can influence the electrode utilization changed from 0.79% to 0.98%.

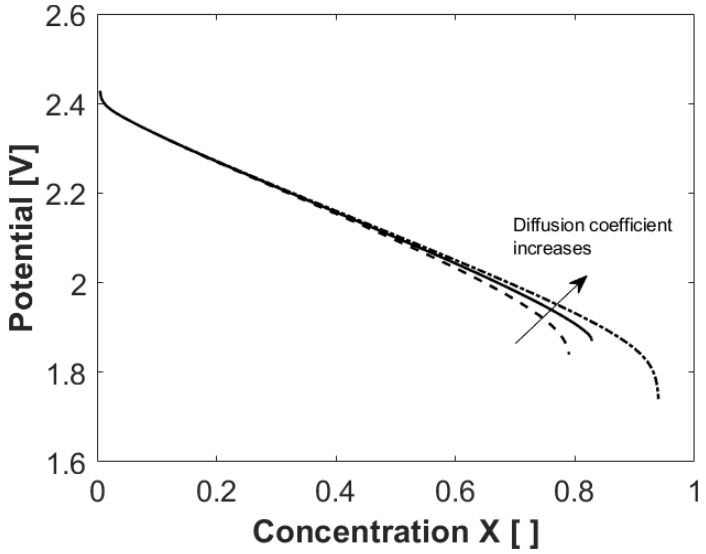

Figure 21: *Effect of cation diffusion coefficient on the battery performance.*

5.3.1 Contact Resistance

Figure 22 shows the effect of the percentage of contact resistance (defined in the method section). Results show that the contact resistance has minimal influence on the electrode utilization. The simulation results revealed that the contact resistance influences the battery voltage. More resistance requires more voltage to maintain the same flux of ions (same current) during the battery operation. However, the increase in voltage is small, changing from 1.93 to 1.95 V. These results imply that a drop in the concentration arising from the contact resistance may not significantly influence the performance. Still, a contact resistance above 100% percent is not physically possible, and must be carefully considered to avoid reaching the maximum allowed limit of 100% contact resistance.

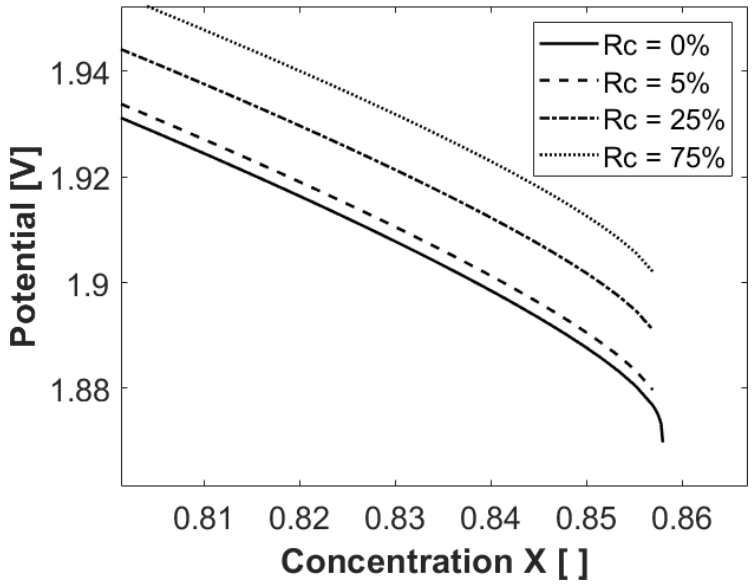

Figure 22: *Effect of contact resistance on the battery performance*

6.0 Limitations

Due to the limitations of the test equipment and techniques available, it was not possible to reliably measure the solid component material properties such as the conductivity and porosity of the individual cathode or electrolyte. For example, the individual cathode or electrolyte pellets often crumbled before an attempt to test or image. This is because free standing pellets needed to be created outside of the contained small peek tube (Figure 9) in order to be tested. As a result, the lack of lateral support greatly weakened the material integrity. Another issue is that the dye used to create the free-standing pellet needed to be lubricated prior to use. Because the cathode and electrode powder came in contact with the lubricant while being pressed, there is ambiguity about the final chemical composition of the materials.

The verification of the model developed in Ansys-Fluent was done through direct comparison with the results reported by West et al. [22]. The West model is based on the experimental parameters

of a battery cell with a titanium disulfide cathode and LiClO4/PC (lithium perchlorate dissolved in propylene carbonate) electrolyte. All of the pertinent equations in West's model describe the transport of ion transport across the electrode and electrolyte in a lithium battery. However, due to the difference in cathode material used for the model (titanium disulfide) and experiment (NMC composite), the voltage for the model and experimental cell could not be directly compared. Therefore, the model in Ansys-Fluent still needs to be adjusted for direct comparison with the experimental data to achieve a fully validated model.

6.1 Future Work

It is necessary to improve the current experimental techniques for measuring SSB performance. First, a more reliable way of creating a free-standing pellet needs to be developed. The method used should not affect the chemical composition of the pellet while also maintaining the structural integrity of the pressed powder. To accomplish this, an extensive literature review should be conducted to evaluate the current methods being used to conduct performance measurements of individual SSB layers. Finding a reliable method of testing will enable the necessary SSB experimental parameters to be collected to achieve a more sophisticated characterization of the battery performance. In the current study, the fabrication pressure and cathode composition were studied as independent variables. Improving testing methods would also help identify if there is a correlation between the pressure and composition for battery cycling stability.

So far, the model the model is only able to simulate discharge of the battery. Further development is required to model the charge process. This can be done by identifying the necessary transport mechanisms in the electrode and electrolyte. Also, it is important to identify the correct condition

for the lithium-ion reaction at the electrode/electrolyte interface. A complete model, including the discharge and charge process, can be useful for investigating material degradation. In addition, the complete model can be utilized to identify the main parameters contributing to battery performance. Another possible improvement lies in identifying the relation between contact resistance and current density losses. This relation can be identified by conducting controlled experiments using different electrode materials and fabrication pressures.

6.2 Conclusions

Batteries are important because they are necessary to store and provide energy to a multitude of portable devices. Batteries can also be used to advance renewable energy generation by providing a reliable method of energy storage. In order to provide these tasks more sustainably and efficiently, the current energy density limits of conventional li-ion batteries must be surpassed. One rising solution is the use of solid-state batteries which have great energy density potential. The main limitation to SSBs is material instability. The cathode analyzation results determine that the NMC composite cathodes are a strong match for sulfide solid electrolytes. This is evident through the material ratio testing done in section 5.1. In Figure 12, the minimum resistance was found to be 380 ohms for a composite cathode material ratio of 76:19:5 = NMC: LPSCL:Carbon black. Decreasing the amount of cathode active material (NMC) by 16 percent increased cell resistance to a maximum of 650 ohms (Figure 14). Despite this increase in resistance the best cycling stability was shown at the lower NMC ratio. This is best indicated by the cycling results shown in Figure 19 which showed minimal decay over a five-day cycle, indicating great stability between the SE and cathode. The five-day cycling result was achieved at a fabrication pressure of

25 MPa.

The study considered four key hypotheses as a baseline. The obtained results indicated:

Hypothesis 1: **Solid material ratio composition affects battery resistance influencing performance.** The cathode optimization results determine that the NMC composite cathodes are a strong match for sulfide solid electrolytes. This is evident through the material ratio testing done in section 5.1. In Figure 12, the minimum resistance was found to be 380 ohms for a composite cathode material ratio of 76:19:5 = NMC: LPSCL: Carbon black. Decreasing the amount of cathode active material (NMC) by 16 percent increased cell resistance to a maximum of 650 ohms (Figure 14). Despite this increase in resistance the best cycling stability was shown at the lower NMC ratio. This indicates that, for an NMC composite cathode and LPSCL solid electrolyte, there is potential for improved performance using a more balanced ratio of 60 % cathode active material (NMC) to 35 % conductive additive (LPSCL).

Hypothesis 2: **Fabrication pressure affects cycling stability.** The study showed that fabrication pressure has a strong influence on the battery cycling time. The cycling time varied in the range of 4 hours to 5 days. The range of fabrication pressures that reflected these results were 350, 50, 2.5, and 25 MPa. Each pressure was tested twice to allow for any significant change in the cycle time result to be captured. Out of all the pressures tested, the best performance was obtained with a fabrication pressure of 25 MPa. This is best indicated by the cycling results shown in Figure 19 which showed minimal decay over a five-day cycle, indicating great stability between the SE and cathode.

Hypothesis 3: **Ion diffusion coefficient affects battery performance.** The simulation model allowed identifying the effect of the cation diffusion coefficient. Results indicated that the diffusion

coefficient influences the utilization of the electrode. A higher diffusion coefficient allows a strong transport of ions to the electrode/electrolyte interface leading to longer operation times. Another factor that affects electrode utilization is cathode composition. It is necessary for the cathode material to allow ions to freely pass into the electrode, otherwise the ions will stay in the electrolyte and the battery will not fully charge and discharge leading to shorter cycle times. Therefore, the results of this model imply that the reason for the rapid decay in cycling of the 76:19:5 ratio vs. the 60:35:5 ratio is that the electrode was not able to accept all of the ions in the electrolyte when the battery was discharged.

Hypothesis 4: **Contact resistance affects the performance of the battery.** The proposed approach modeled contact resistance assuming conservation of current and a drop in the ionic concentration. The results revealed that the contact resistance has a minimal influence on the electrode or electrolyte utilization. It affects the voltage of the battery up to 0.02 V. Still, the contact resistance can lead to a significant drop in the concentration going above the limit of the drop in the electrode, which can lead to battery failure. The effect of battery failure caused by contact resistance is shown in the soft shorts that occurred during the cycling of fabrication pressure tests #1-3. The soft short in test #1 and 2 implies that the pressure (350 MPa) was too high and damaged the cell creating contact loss along the interface. The soft short at the low pressure used for test #3 (2.5 MPa) implies that the cathode pellet formed did not have full surface contact with the electrolyte. Similarly, the battery model identified a short when the contact resistance exceeded the electrode resistance. These results imply that contact resistance is a primary factor being influenced by the changes in the fabrication pressure.

The creation of an electrochemically stable relationship between the NMC composite cathode and sulfide solid electrolyte is significant because it allows the potential capacity of the lithium anode

to be maximized. The higher that the capacity of the cathode can reach while remaining stable, the greater the chance for reaching the energy density potential of SSBs. Given the novelty of SSBs analyzation techniques, refinement of different material ratios and fabrication techniques must continue to grow along with battery performance.

Acknowledgement

I hereby gratefully acknowledge the permission granted by Professor Howard Tu to use the collected data during my tenure at the Clean Energy and Water Laboratory at RIT.

References

[1] J. Alarco, P. Talbot, and T. Conversation, “The history and development of batteries.” Accessed: Dec. 14, 2023. [Online]. Available: https://phys.org/news/2015-04-history-batteries.html

[2] Y. Chen *et al.*, “A review of lithium-ion battery safety concerns: The issues, strategies, and testing standards,” *Journal of Energy Chemistry*, vol. 59, pp. 83–99, Aug. 2021, doi: 10.1016/j.jechem.2020.10.017.

[3] M. V. Reddy, A. Mauger, C. M. Julien, A. Paolella, and K. Zaghib, “Brief History of Early Lithium-Battery Development,” *Materials (Basel)*, vol. 13, no. 8, p. 1884, Apr. 2020, doi: 10.3390/ma13081884.

[4] K. Schmidt-Rohr, “How Batteries Store and Release Energy: Explaining Basic Electrochemistry,” *J. Chem. Educ.*, vol. 95, no. 10, pp. 1801–1810, Oct. 2018, doi: 10.1021/acs.jchemed.8b00479.

[5] A. Hamidi, E. Manla, and A. Nasiri, “Li-ion batteries and Li-ion ultracapacitors: Characteristics, modeling and grid applications,” Sep. 2015, pp. 4973–4979. doi: 10.1109/ECCE.2015.7310361.

[6] T. M. Bandhauer, S. Garimella, and T. F. Fuller, “A Critical Review of Thermal Issues in Lithium-Ion Batteries,” *J. Electrochem. Soc.*, vol. 158, no. 3, p. R1, Jan. 2011, doi: 10.1149/1.3515880.

[7] J. Janek and W. G. Zeier, “Challenges in speeding up solid-state battery development,” *Nat Energy*, vol. 8, no. 3, Art. no. 3, Mar. 2023, doi: 10.1038/s41560-023-01208-9.

[8] F. Hao, F. Han, Y. Liang, C. Wang, and Y. Yao, “Architectural design and fabrication approaches for solid-state batteries,” *MRS Bull.*, vol. 43, no. 10, pp. 775–781, Oct. 2018, doi: 10.1557/mrs.2018.211.

[9] M. Kotobuki, K. Kanamura, Y. Sato, and T. Yoshida, “Fabrication of all-solid-state lithium battery with lithium metal anode using Al2O3-added Li7La3Zr2O12 solid electrolyte,” *Journal of Power Sources*, vol. 196, no. 18, pp. 7750–7754, Sep. 2011, doi: 10.1016/j.jpowsour.2011.04.047.

[10] S. Hess, M. Wohlfahrt-Mehrens, and M. Wachtler, “Flammability of Li-Ion Battery Electrolytes: Flash Point and Self-Extinguishing Time Measurements,” *J. Electrochem. Soc.*, vol. 162, no. 2, p. A3084, Jan. 2015, doi: 10.1149/2.0121502jes.

[11] Y. Guo *et al.*, “Solid-state lithium batteries: Safety and prospects,” *eScience*, vol. 2, no. 2, pp. 138–163, Mar. 2022, doi: 10.1016/j.esci.2022.02.008.

[12] S. Anenberg, “A global snapshot of the air pollution-related health impacts of transportation sector emissions in 2010 and 2015”.

[13] G. Mullally *et al.*, *A Roadmap for Local Deliberative Engagements on Transitions to Net Zero Carbon and Climate Resilience*. 2022. doi: 10.13140/RG.2.2.35125.35048.

[14] L. Guo, J. Zheng, L. Zhao, and Y. Yao, “Interfacial instabilities in halide-based solid-state batteries,” *MRS Bull.*, Oct. 2023, doi: 10.1557/s43577-023-00607-3.

[15] P. Minnmann *et al.*, “Designing Cathodes and Cathode Active Materials for Solid-State Batteries,” *Advanced Energy Materials*, vol. 12, no. 35, p. 2201425, 2022, doi: 10.1002/aenm.202201425.

[16] H.-W. Zhang *et al.*, “Understanding and Predicting the Lithium Dendrite Formation in Li-Ion Batteries: Phase Field Model,” *ECS Trans.*, vol. 61, no. 8, p. 1, Sep. 2014, doi: 10.1149/06108.0001ecst.

[17] R. Koerver *et al.*, “Capacity Fade in Solid-State Batteries: Interphase Formation and Chemomechanical Processes in Nickel-Rich Layered Oxide Cathodes and Lithium Thiophosphate Solid Electrolytes,” *Chem. Mater.*, vol. 29, no. 13, pp. 5574–5582, Jul. 2017, doi: 10.1021/acs.chemmater.7b00931.

[18] M. Esmaeilpour, S. Jana, H. Li, M. Soleymanibrojeni, and W. Wenzel, “A Solution-Mediated Pathway for the Growth of the Solid Electrolyte Interphase in Lithium-Ion Batteries,” *Advanced Energy Materials*, vol. 13, no. 14, p. 2203966, 2023, doi: https://doi.org/10.1002/aenm.202203966.

[19] C. Hänsel and D. Kundu, “The Stack Pressure Dilemma in Sulfide Electrolyte Based Li Metal Solid-State Batteries: A Case Study with Li6PS5Cl Solid Electrolyte,” *Advanced Materials Interfaces*, vol. 8, no. 10, p. 2100206, 2021, doi: 10.1002/admi.202100206.

[20] J. E. Vogel *et al.*, "Li-Ion Battery Electrode Contact Resistance Estimation by Mechanical Peel Test," *J. Electrochem. Soc.*, vol. 169, no. 8, p. 080508, Aug. 2022, doi: 10.1149/1945-7111/ac8504.
[21] S. Randau *et al.*, "Benchmarking the performance of all-solid-state lithium batteries," *Nat Energy*, vol. 5, no. 3, Art. no. 3, Mar. 2020, doi: 10.1038/s41560-020-0565-1.
[22] S. Y. Han *et al.*, "Stress evolution during cycling of alloy-anode solid-state batteries," *Joule*, vol. 5, no. 9, pp. 2450–2465, Sep. 2021, doi: 10.1016/j.joule.2021.07.002.
[23] N. Suzuki *et al.*, "Highly Cyclable All-Solid-State Battery with Deposition-Type Lithium Metal Anode Based on Thin Carbon Black Layer," *Advanced Energy and Sustainability Research*, vol. 2, no. 11, p. 2100066, 2021, doi: 10.1002/aesr.202100066.
[24] Y. Zhang *et al.*, "High-capacity, low-tortuosity, and channel-guided lithium metal anode," *Proceedings of the National Academy of Sciences*, vol. 114, no. 14, pp. 3584–3589, Apr. 2017, doi: 10.1073/pnas.1618871114.
[25] J. A. Lewis, J. Tippens, F. J. Q. Cortes, and M. T. McDowell, "Chemo-Mechanical Challenges in Solid-State Batteries," *Trends in Chemistry*, vol. 1, no. 9, pp. 845–857, Dec. 2019, doi: 10.1016/j.trechm.2019.06.013.
[26] J. Wang, Y.-S. He, and J. Yang, "Sulfur-Based Composite Cathode Materials for High-Energy Rechargeable Lithium Batteries," *Advanced Materials*, vol. 27, no. 3, pp. 569–575, 2015, doi: 10.1002/adma.201402569.
[27] J. Park *et al.*, "Dimension-controlled solid oxide electrolytes for all-solid-state electrodes: Percolation pathways, specific contact area, and effective ionic conductivity," *Chem. Eng. J.*, vol. 391, p. 123528, Jul. 2020, doi: 10.1016/j.cej.2019.123528.
[28] C. Wang, J. Liang, Y. Zhao, M. Zheng, X. Li, and X. Sun, "All-solid-state lithium batteries enabled by sulfide electrolytes: from fundamental research to practical engineering design," *Energy Environ. Sci.*, vol. 14, no. 5, pp. 2577–2619, May 2021, doi: 10.1039/D1EE00551K.
[29] J. Wang and F. Hao, "Experimental Investigations on the Chemo-Mechanical Coupling in Solid-State Batteries and Electrode Materials," *Energies*, vol. 16, no. 3, p. 1180, Feb. 2023, doi: 10.3390/en16031180.
[30] P. Bonnick, K. Niitani, M. Nose, K. Suto, T. S. Arthur, and J. Muldoon, "A high performance all solid state lithium sulfur battery with lithium thiophosphate solid electrolyte," *J. Mater. Chem. A*, vol. 7, no. 42, pp. 24173–24179, Oct. 2019, doi: 10.1039/C9TA06971B.
[31] C. Dietrich *et al.*, "Spectroscopic characterization of lithium thiophosphates by XPS and XAS - a model to help monitor interfacial reactions in all-solid-state batteries," *Phys. Chem. Chem. Phys.*, vol. 20, no. 30, pp. 20088–20095, Aug. 2018, doi: 10.1039/c8cp01968a.
[32] L. Zhao, A. E. Lakraychi, Z. Chen, Y. Liang, and Y. Yao, "Roadmap of Solid-State Lithium-Organic Batteries toward 500 Wh kg–1," *ACS Energy Lett.*, vol. 6, no. 9, pp. 3287–3306, Sep. 2021, doi: 10.1021/acsenergylett.1c01368.
[33] K. B. Hatzell *et al.*, "Challenges in Lithium Metal Anodes for Solid-State Batteries," *ACS Energy Lett.*, vol. 5, no. 3, pp. 922–934, Mar. 2020, doi: 10.1021/acsenergylett.9b02668.
[34] S. Sarkar and V. Thangadurai, "Critical Current Densities for High-Performance All-Solid-State Li-Metal Batteries: Fundamentals, Mechanisms, Interfaces, Materials, and Applications," *ACS Energy Lett.*, vol. 7, no. 4, pp. 1492–1527, Apr. 2022, doi: 10.1021/acsenergylett.2c00003.
[35] V. Raj, N. P. B. Aetukuri, and J. Nanda, "Solid state lithium metal batteries – Issues and challenges at the lithium-solid electrolyte interface," *Current Opinion in Solid State and Materials Science*, vol. 26, no. 4, p. 100999, Aug. 2022, doi: 10.1016/j.cossms.2022.100999.
[36] A. Desrues *et al.*, "Electrochemical and X-ray Photoelectron Spectroscopic Study of Early SEI Formation and Evolution on Si and Si@C Nanoparticle-Based Electrodes," *Materials (Basel)*, vol. 15, no. 22, p. 7990, Nov. 2022, doi: 10.3390/ma15227990.
[37] Y. Wang *et al.*, "Design principles for solid-state lithium superionic conductors," *Nature Mater*, vol. 14, no. 10, Art. no. 10, Oct. 2015, doi: 10.1038/nmat4369.
[38] W. Fitzhugh, X. Chen, Y. Wang, L. Ye, and X. Li, "Solid–electrolyte-interphase design in constrained ensemble for solid-state batteries," *Energy & Environmental Science*, vol. 14, no. 8, pp. 4574–4583,

2021, doi: 10.1039/D1EE00754H.
[39] K. Kerman, A. Luntz, V. Viswanathan, Y.-M. Chiang, and Z. Chen, “Review—Practical Challenges Hindering the Development of Solid State Li Ion Batteries,” *J. Electrochem. Soc.*, vol. 164, no. 7, p. A1731, Jun. 2017, doi: 10.1149/2.1571707jes.
[40] T. Mageto, S. D. Bhoyate, F. M. de Souza, K. Mensah-Darkwa, A. Kumar, and R. K. Gupta, “Developing practical solid-state rechargeable Li-ion batteries: Concepts, challenges, and improvement strategies,” *Journal of Energy Storage*, vol. 55, p. 105688, Nov. 2022, doi: 10.1016/j.est.2022.105688.
[41] L. Ye and X. Li, “A dynamic stability design strategy for lithium metal solid state batteries,” *Nature*, vol. 593, no. 7858, Art. no. 7858, May 2021, doi: 10.1038/s41586-021-03486-3.
[42] L. Albero Blanquer *et al.*, “Optical sensors for operando stress monitoring in lithium-based batteries containing solid-state or liquid electrolytes,” *Nat Commun*, vol. 13, no. 1, Art. no. 1, Mar. 2022, doi: 10.1038/s41467-022-28792-w.
[43] K. West, T. Jacobsen, and S. Atlung, “Modeling of Porous Insertion Electrodes with Liquid Electrolyte,” *J. Electrochem. Soc.*, vol. 129, no. 7, p. 1480, Jul. 1982, doi: 10.1149/1.2124188.
[44] C. Y. Wang, W. B. Gu, and B. Y. Liaw, “Micro-Macroscopic Coupled Modeling of Batteries and Fuel Cells: I. Model Development,” *J. Electrochem. Soc.*, vol. 145, no. 10, p. 3407, Oct. 1998, doi: 10.1149/1.1838820.
[45] S. T. Taleghani, B. Marcos, K. Zaghib, and G. Lantagne, “A Study on the Effect of Porosity and Particles Size Distribution on Li-Ion Battery Performance,” *J. Electrochem. Soc.*, vol. 164, no. 11, p. E3179, May 2017, doi: 10.1149/2.0211711jes.
[46] V. Müller, R.-G. Scurtu, M. Memm, M. A. Danzer, and M. Wohlfahrt-Mehrens, “Study of the influence of mechanical pressure on the performance and aging of Lithium-ion battery cells,” *Journal of Power Sources*, vol. 440, p. 227148, Nov. 2019, doi: 10.1016/j.jpowsour.2019.227148.
[47] J. S. Horner *et al.*, “Electrochemical Modeling of GITT Measurements for Improved Solid-State Diffusion Coefficient Evaluation,” *ACS Appl. Energy Mater.*, vol. 4, no. 10, pp. 11460–11469, Oct. 2021, doi: 10.1021/acsaem.1c02218.
[48] M. Doyle, T. F. Fuller, and J. Newman, “Modeling of Galvanostatic Charge and Discharge of the Lithium/Polymer/Insertion Cell,” *J. Electrochem. Soc.*, vol. 140, no. 6, p. 1526, Jun. 1993, doi: 10.1149/1.2221597.
[49] T. F. Fuller, M. Doyle, and J. Newman, “Simulation and Optimization of the Dual Lithium Ion Insertion Cell,” *J. Electrochem. Soc.*, vol. 141, no. 1, p. 1, Jan. 1994, doi: 10.1149/1.2054684.
[50] T. S. Chadha, B. Suthar, D. Rife, V. R. Subramanian, and P. Biswas, “Model Based Analysis of One-Dimensional Oriented Lithium-Ion Battery Electrodes,” *J. Electrochem. Soc.*, vol. 164, no. 11, p. E3114, May 2017, doi: 10.1149/2.0141711jes.
[51] D. Chen, J. Jiang, G.-H. Kim, C. Yang, and A. Pesaran, “Comparison of different cooling methods for lithium ion battery cells,” *Applied Thermal Engineering*, vol. 94, pp. 846–854, Feb. 2016, doi: 10.1016/j.applthermaleng.2015.10.015.
[52] M. Mačák, P. Vyroubal, T. Kazda, D. Capkova, and J. Maxa, “Numerical Modelling of Discharging the Lithium-Sulphur Batteries in Ansys Fluent,” *Advances in Military Technology*, vol. 17, no. 2, Art. no. 2, Aug. 2022, doi: 10.3849/aimt.01525.
[53] M. P. Parmar, D. R. Patel, V. K. Patel, and R. S. Patel, “Thermal Simulation of Li-Ion Battery Pack Using ANSYS Fluent,” in *Recent Advances in Mechanical Infrastructure*, A. K. Parwani, PL. Ramkumar, K. Abhishek, and S. K. Yadav, Eds., in Lecture Notes in Intelligent Transportation and Infrastructure. Singapore: Springer, 2021, pp. 265–274. doi: 10.1007/978-981-33-4176-0_22.
[54] L. Cai and R. White, “Mathematical Modeling of a Lithium Ion Battery,” in *Proceedings of the COMSOL Conference*, Boston, 2009.
[55] I. Perez-Raya and S. G. Kandlikar, “Chapter Three - Evaporation on a Planar Interface – Numerical Simulation and Theoretical Analysis of Heat and Mass Transport Processes,” in *Advances in Heat Transfer*, vol. 48, E. M. Sparrow, J. P. Abraham, J. M. Gorman, T. F. Irvine, and J. P. Hartnett, Eds., Elsevier, 2016, pp. 125–190. doi: 10.1016/bs.aiht.2016.08.005.